Developments in the Built Environment 17 (2024) 100343

Contents lists available at ScienceDirect

Developments in the Built Environment

journal homepage: www.sciencedirect.com/journal/developments-in-the-built-environment

Strain-hardening effect on the flexural behavior of ultra-high-performance fiber-reinforced concrete beams with steel rebars

Doo-Yeol Yoo [a], Salman Soleimani-Dashtaki [b], Taekgeun Oh [a], Booki Chun [c], Nemkumar Banthia [b], Seung-Jung Lee [d,*], Young-Soo Yoon [e,**]

[a] Department of Architecture and Architectural Engineering, Yonsei University, 50 Yonsei-ro, Seodaemun-gu, Seoul, 03722, Republic of Korea
[b] Department of Civil Engineering, The University of British Columbia, 6250 Applied Science Lane, Vancouver, BC, V6T 1Z4, Canada
[c] Department of Architectural Engineering, Hanyang University, 222 Wangsimni-ro, Seongdong-gu, Seoul, 04763, Republic of Korea
[d] Department of Civil and Environmental Engineering, Incheon National University, 119 Academy-ro, Yeonsu-gu, Incheon, 22012, Republic of Korea
[e] School of Civil, Environmental and Architectural Engineering, Korea University, 145 Anam-ro, Seongbuk-gu, Seoul, 02841, Republic of Korea

ARTICLE INFO

Keywords:
Ultra-high-performance fiber-reinforced concrete
Steel fiber effect
Tensile characteristics
Ductility
Fiber orientation coefficient
Inverse analysis

ABSTRACT

This study evaluated the effects of volume fraction, aspect ratio, and shape of steel fibers on the mechanical properties of ultra-high-performance fiber-reinforced concrete (UHPFRC) and the structural behavior of reinforced (R-) UHPFRC beams. The tensile strength and energy absorption capacity of ultra-high-performance concrete (UHPC) are improved by adding steel fibers and increasing its volume contents by up to 3.0 %. Compared with short straight steel fiber, medium-length straight and twisted fibers at a volume fraction of 2.0 % result in twice higher energy absorption capacity and higher flexural strength of R–UHPFRC beams. The flexural strength of R–UHPC beams increases by increasing the fiber content up to 3.0 %. However, the strain-hardening characteristics of UHPFRC negatively influence the cracking behavior and stress redistribution in structural beams, causing 48.2–54.1 % lower ultimate ductility indices. The small amounts of steel fibers with volume fraction of ≤1.0 % that exhibit strain-softening behavior only improve the peak ductility.

1. Introduction

Owing to the excellent tensile strength and ductility of ultra-high-performance fiber-reinforced concrete (UHPFRC), introduced by Richard and Cheyrezy (1995), its practical applications in civil infrastructures and buildings as flexural members have attracted the attention of structural engineers (Feng et al., 2021; Hung and Chueh, 2016; Sawicki et al., 2022; Zhou et al., 2022; Shao and Ostertag, 2022). As the steel fibers incorporated in ultra-high-performance concrete (UHPC) can withstand only a portion of the tensile load at the crack surfaces, an additional tensile stress block in the section is considered, which generally increases the moment capacity of reinforced UHPC beams (Yoo and Yoon, 2015). In addition, the excellent bond strength between the steel reinforcing bar (rebar) and UHPFRC results in a substantially lower development length (approximately 20–30 % of that in ordinary concrete) (Ronanki et al., 2018). Previously, a steel rebar with a yield strength of 522.7 MPa was obtained after it was embedded in UHPFRC with an embedment length of two times the rebar diameter, given a sufficient cover depth (Yoo et al., 2015a). This allows the easy use of steel rebars in UHPFRC members by reducing the attention of rebar anchorage design.

Several studies (Yoo and Yoon, 2015; Saqif et al., 2022; Yang et al., 2010; Chen et al., 2018; Qiu et al., 2022; Yoo et al., 2016a; Feng et al., 2022; Shao and Billington, 2022) have been conducted to evaluate the flexural behavior of reinforced (R-)UHPFRC beams that have various reinforcement ratios and volume fractions of discontinuous fibers. Yang et al. (2010) investigated the effects of the rebar ratio (0–1.96 %) and placement method on the flexural behavior of R–UHPFRC beams with a constant fiber volume fraction (V_f) of 2 %. They reported that a ductility index greater than 1.6 was maintained for the R–UHPFRC beams and that it generally increased with an increase in rebar ratio. The fiber orientation and arrangement were influenced by the placement method, and a better flexural performance resulted from placing the UHPFRC at the beam end rather than at the mid-span. The presence of steel fibers (V_f of 2 %) is effective in improving the moment capacity, post-cracking stiffness, and cracking response of the R–UHPC beams; however, it

* Corresponding author.
** Corresponding author.
E-mail addresses: seungjung@inu.ac.kr (S.-J. Lee), ysyoon@korea.ac.kr (Y.-S. Yoon).

https://doi.org/10.1016/j.dibe.2024.100343
Received 17 October 2023; Received in revised form 11 December 2023; Accepted 19 January 2024
Available online 26 January 2024

decreases their ductility (Yoo and Yoon, 2015). Further, increasing of the straight steel fiber length and using twisted steel (TS) fibers improves the post-peak response and ductility of R–UHPFRC beams. Based on numerical analysis, Yoo and Yoon (2015) concluded that the adoption of a fiber orientation coefficient (K) of 1.25, as per the AFGC Interim Recommendations (AFGC, 2013), yields a better prediction than that without considering K, because of the different fiber distribution characteristics between the small prismatic beams used for inverse analysis and the large structurally reinforced beams. Chen et al. (2018) found that the flexural capacity and ductility of R–UHPFRC beams, which included 2 % 13-mm-long SS fibers, were influenced by the reinforcement ratio. The flexural capacity increased as the reinforcement ratio was raised from 1.09 % to 4.99 %. However, the highest ductility indices were obtained at certain reinforcement ratios. To predict the ultimate moment capacity of R–UHPFRC beams, they (Chen et al., 2018) suggested a tensile strength coefficient of 0.47 for an equivalent tensile stress block. According to a study performed by Saqif et al. (2022), an increase in material ductility does not necessarily enhance the ductility of R–UHPFRC beams at low reinforcement ratios of 0.85 % and 1.54 %, and a decrease in reinforcement ratio leads to an increase in the reinforced beam ductility. Saqif et al. (2022) suggested that a V_f between 1.0 % and 1.5 % is appropriate for the fabrication of R–UHPFRC beams with low reinforcement ratios. Shao and Billington (2022) examined the synergistic impacts of steel fiber volume fractions (0.5–2.0 %) and longitudinal rebar ratios (0.96 % and 2.10 %). They (Shao and Billington, 2022) found that reducing the tensile strength of UHPFRC, increasing the steel rebar ratio, and enhancing the post-yield hardening strength of steel rebar are effective strategies for enhancing drift capacity. Moreover, these measures alter the failure path of flexural elements, shifting from crack localization to failure after gradual strain hardening.

Naaman and Reinhardt (2006) classified fiber-reinforced cement (FRC) composites as tensile strain-softening or -hardening composites. The strain-hardening composites provide a higher load-carrying capacity in tension after a formation of matrix percolation cracks, thus exhibiting multiple-crack patterns, whereas the strain-softening composites develop single-crack widening with softening behavior after the initiation of matrix crack. The fiber bridging capacity, which is a main factor affecting the post-cracking tensile response, is influenced by the volume content of the fibers (Yoo et al., 2017a). Therefore, depending on the steel fiber content, either strain-softening or -hardening of the UHPFRC composites under tension can be achieved (Wille et al., 2011). According to Wille et al. (2011), UHPFRC with short straight (SS) steel fibers (l_f, 13 mm) in volume fraction of 1.5 % or higher lead to the tensile strain-hardening behavior ($\sigma_{pc} \geq \sigma_{cc}$), where l_f is the fiber length, σ_{pc} is the post-cracking tensile strength, and σ_{cc} is the initial cracking tensile strength. As strain-softening and -hardening composites exhibit different cracking patterns, the structural ductility of R–UHPFRC is expected to be affected by the tensile characteristics of the material. Although a few studies (Saqif et al., 2022; Shao and Billington, 2022) have evaluated the effect of steel fiber content on the ductility of R–UHPFRC beams, published studies evaluating the structural ductility according to the material tensile characteristics, such as strain softening versus strain hardening, are currently lacking. Accordingly, in this study, various steel fiber volume fractions, ranging from very low (0.5 %) to high (3.0 %), were considered to produce strain-softening and -hardening UHPFRC composites; subsequently, their impact on the flexural behavior of R–UHPFRC beams was evaluated.

The AFGC recommendations (AFGC, 2013) suggest using a fiber orientation coefficient, K, to consider the random orientation of the fibers. However, the coefficient K must be changed according to various factors, such as the fiber volume fraction, aspect ratio, shape, cross-sectional dimensions, and casting method. Yoo et al. (2017b) reported that the coefficient K increases with increasing cross-sectional area of reinforced concrete beams. Therefore, the effect of the fiber reinforcing index (FRI), which considers both the fiber volume fraction and aspect ratio, on the fiber orientation coefficient K must be investigated simultaneously. To this end, finite element (FE) analysis was performed by considering the material models suggested from the experiments to predict the behavior of R–UHPFRC beams under flexure, and by inverse analysis, an appropriate coefficient K was suggested as a function of the FRI.

Table 1
Mix proportion of UHPC.

W/B	Mix design [kg/m^3]					
	Water	Cement	Silica fume	Silica flour	Silica sand	Superplasticizer[a]
0.2	160.3	788.5	197.1	236.6	867.4	52.6

[Note] UHPC = ultra-high-performance concrete and W/B = water-to-binder ratio.
[a] Superplasticizer includes 30 % solid (=15.8 kg/m^3) and 70 % water (=36.8 kg/m^3).

2. Research significance

The demand for R–UHPFRC structures has been increasing, leading to extensive studies conducted on this topic. Since UHPFRC exhibits superior tensile strength and energy absorption capacity, researchers have been particularly interested in its applications in tensile or flexural members. Most studies have focused on assessing the flexural behavior of R–UHPFRC beams with varying longitudinal steel rebar ratios, emphasizing high steel fiber volume fractions. However, only a limited number of studies have considered low steel fiber volume fractions below 1.0 %. The tensile behavior of UHPFRC significantly influences the structural performance of R–UHPFRC beams, and it is highly dependent on the steel fiber volume fractions. Therefore, this study investigates the effects of steel fiber volume fractions ranging from low to high (0.5 %–3.0 %). The study evaluates the impact of tensile strain-hardening and -softening characteristics on the ductility of R–UHPFRC beams. Additionally, for an accurate prediction of the flexural behavior of R–UHPFRC beams, the fiber orientation factor (K) must be considered. Fiber orientation is influenced by the FRR, and thus, this study first examines the changes in the factor K according to the FRI.

3. Test program

3.1. Fabrications of UHPC and UHPFRC

According to ACI Committee 239 (ACI Committee 239, 2012), UHPC is suggested as a concrete material with a minimum specified compressive strength of 150 MPa and specified durability, tensile ductility, and toughness requirements. Discontinuous fibers are generally included to meet specified requirements. Thus, to achieve such an ultrahigh strength, a very low water-to-binder (W/B) ratio of 0.2 was adopted, including 70 % water from the polycarboxylate superplasticizer (SP). As a binding material, type I ordinary Portland cement and silica fume with mean grain sizes of 11.43 and 0.20 μm, respectively, were used. In addition, silica sand and flour with mean grain sizes of 236.24 and 6.75 μm were used as fine aggregate and filler to increase

Table 2
Geometrical and physical properties of SS, MS, and TS fibers.

Fiber type	Diameter, d_f [mm]	Length, l_f [mm]	Aspect ratio [l_f/d_f]	Density [g/cm^3]	Tensile strength [MPa]	Elastic modulus [GPa]
SS	0.2	13	65.0	7.9	2,788	200
MS	0.2	19.5	97.5	7.9	2,500	200
TS	0.3	30.0	100.0	7.9	2,428	200

[Note] SS = short straight steel fiber, MS = medium length straight steel fiber, and TS = twisted steel fiber.

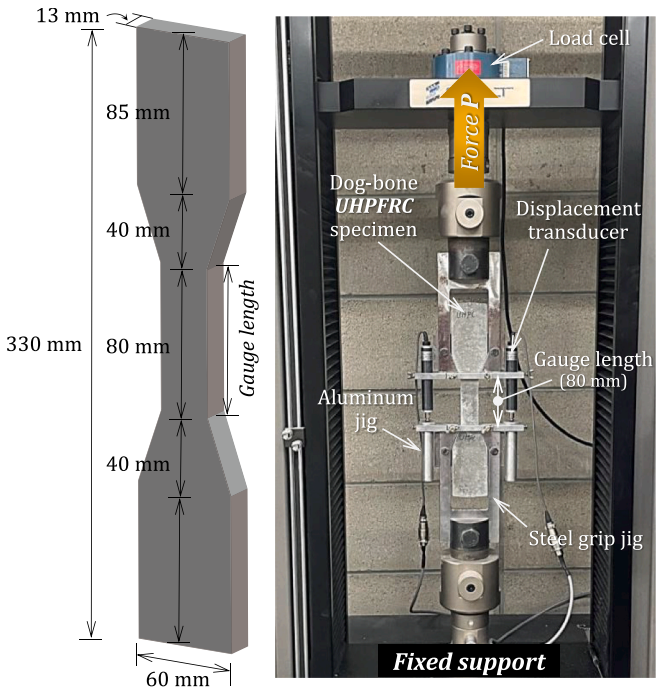

Fig. 1. Direct tensile test setup.

density of matrix, respectively. Owing to the addition of SP, the UHPC was a type of self-consolidating concrete with a flow value of approximately 250 mm. The details of the mix proportions of the UHPC are provided in Table 1.

To evaluate the effects of steel fiber content and type on the tensile behavior of UHPC, three types of steel fibers, namely SS, medium-length straight steel (MS), and TS steel fibers, were used. Their properties are listed in Table 2. For the SS fibers, five volume fractions, ranging from 0.5 % to 3 %, were considered to achieve both strain-softening and strain-hardening behaviors under tension. The steel fiber-doped UHPC is designated as UHPFRC. An identical fiber volume fraction of 2 % was used for the MS and TS fibers. The designation of the test variables was determined by the type and volume fraction of the fiber. For example, specimen SSU2.0 denotes the UHPFRC with 2.0 % (by volume) SS fibers.

The cylindrical and dog-bone specimens for mechanical property evaluation, and the reinforced UHPC and UHPFRC beams for structural behavior evaluation were fabricated using a Hobart-type lab mixer with a capacity of 1,200 L. All dry ingredients were initially added to the mixer and premixed for 10 min to ensure sufficient dispersion. Subsequently, a mixture of water and SP was added and mixed for 10 min to form a flowable UHPC mixture, which was then used to fabricate the UHPC specimens and beams. For the UHPFRC, SS, MS, and TS fibers were carefully added to the mixer and mixed for additional 5 min to achieve fiber dispersion. As the fiber orientation of UHPFRC is strongly dependent on the casting method (Zhou and Uchida, 2017; Yoo et al., 2014a, 2016b; Martinie et al., 2015), all specimens and beams were cast parallel to their longitudinal direction.

To achieve sufficient strength, all specimens and beams were subjected to steam-heat curing. After casting the fresh concrete mixture, the samples were initially cured in a laboratory for 48 h and then demolded. Next, special steam-heat curing at a temperature of 90 °C and relative humidity of over 95 % was applied for 3 d. Subsequently, the samples were stored outside until testing was conducted.

3.2. Mechanical property evaluation

For obtaining fundamental data, the compressive strengths of UHPC and UHPFRC were determined using cylindrical specimens measuring 100 mm in diameter and 200 mm in height. Three specimens were used for each variable to determine the average strength. A universal testing machine was used, and a uniaxial load was monotonically applied to the specimen until failure. The load was recorded using a load cell, and the compressive strength was calculated by dividing the maximum load by the cross-sectional area of the cylinder.

Dog-bone-shaped specimens were fabricated and tested to evaluate their tensile behavior, as per the JSCE recommendations (JSCE, 2008). The specimens utilized had cross-sectional dimensions of 13 mm × 30 mm and a gauge length of 80 mm. To ensure consistent fiber orientation, each specimen was cast with fresh UHPFRC parallel to the longitudinal direction. As shown in Fig. 1, the specimen was inserted into a steel grip jig, and an aluminum frame with two displacement transducers was affixed to the specimen. A fixed-fixed support system was used. A uniaxial tensile force was applied at a rate of 0.4 mm/min, and the force and displacement were simultaneously recorded. The recorded tensile load and displacement were converted to tensile stress and strain by dividing them by the cross-section and gauge length, respectively. Five dog-bone specimens were fabricated and tested for each variable to obtain reliable average values.

3.3. Reinforcing details and test setup of R–UHPC and UHPFRC beams

Fig. 2 shows the geometrical and reinforcement details of reinforced

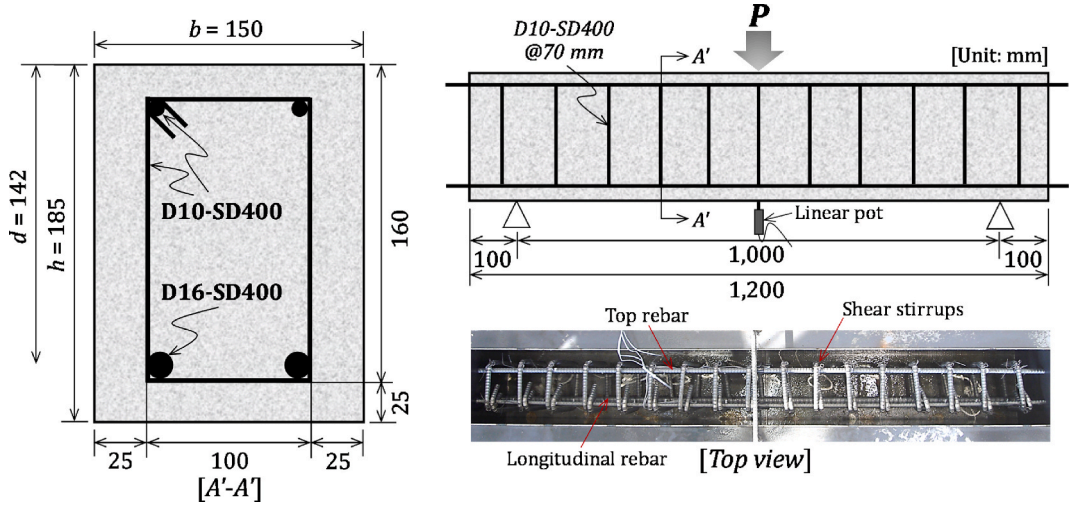

Fig. 2. Cross-sectional and reinforcement details of reinforced UHPC and UHPFRC beams.

Table 3
Properties of steel reinforcing bars.

Designation	Usage	Area [mm^2]	f_y [MPa]	ε_y	f_u [MPa]	ε_u
D10-SD400	Top longitudinal and transverse reinforcements	71.3	549.5	0.0028	667.1	0.0985
D16-SD400	Longitudinal reinforcement	198.6	497.5	0.0025	629.7	0.1149

[Note] f_y = yielding strength, ε_y = yield strain, f_u = ultimate tensile strength, and ε_u = ultimate strain.

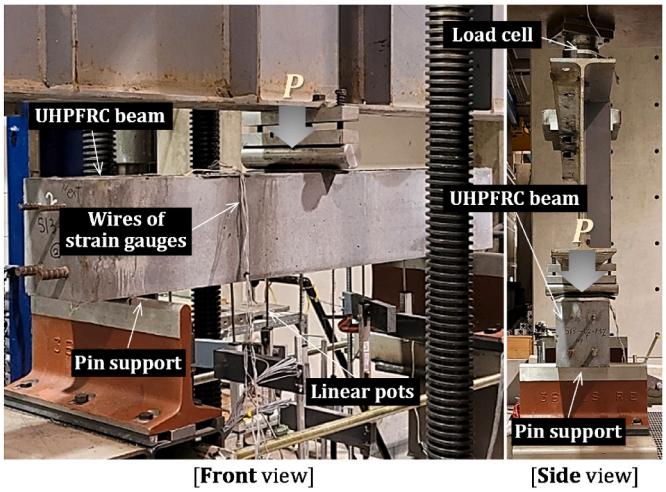

Fig. 3. Setup of structural flexural test for reinforced UHPC and UHPFRC beams.

R–UHPC and R–UHPFRC beams. The cross-sectional dimensions were 150 mm × 185 mm with an effective depth of 142 mm and total length of 1200 mm. Two deformed steel rebars with a diameter of 15.9 mm and cross-sectional area of 198.6 mm^2 were used as longitudinal reinforcements. Thus, the reinforcement ratio was 0.01865. Its yield strength (f_y) and strain (ε_y) were 497.5 MPa and 0.25 %, respectively, and the ultimate strength (f_u) was 629.7 MPa. The mechanical properties of the steel rebars are listed in Table 3. To prevent shear failure, shear stirrups with a diameter of 9.53 mm were applied in a spacing of 70 mm. To install the shear stirrups, a top reinforcement with an identical diameter was also used (Table 3). Yoo and Yoon (2017) reported that the development length of UHPFRC is 2 or 2.5 times the bar diameter of a normal- or high-strength steel rebar, respectively. This implies that the steel rebar embedded in UHPFRC yields before pull-out when its embedded length is greater than twice the bar diameter. Therefore, the longitudinal steel rebars were not bent at the end of the beam but rather extended outside the beam (Fig. 2). The R–UHPFRC beams were manufactured by pouring the fresh UHPFRC mixture in a manner parallel to the longitudinal direction of the beam, akin to the dog-bone specimens.

The detailed setup for the flexural tests of the R–UHPC and R–UHPFRC beams is shown in Fig. 3. A uniaxial load was applied to the center of the beams at a rate of 2 mm/min using a universal testing machine. To prevent the local crushing of concrete at the point load, a rubber pad was placed between the loading pin and top surface of the concrete beams. The beam was placed on a pin support with a clear span length of 1000 mm. To measure the mid-span deflection and deflection shape during testing, seven linear potentiometers (pots) were installed underneath the beam. The locations of the linear pots are shown in Fig. 3. The uniaxial load was applied until the load dropped suddenly owing to the rupture of the longitudinal rebar or compressive crushing of the concrete, which are the general flexural failure modes.

4. Test results and discussion

4.1. Mechanical properties

4.1.1. Compressive strength

As shown in Fig. 4, the average compressive strength of UHPC was influenced by the steel fiber content and type. The average compressive strength for the plain UHPC without steel fibers was 152.5 MPa, which is slightly higher than the required strength value according to ACI Committee 239 (ACI Committee 239, 2012). By incorporating steel fibers, the compressive strength of the UHPC was significantly improved. For example, the highest compressive strength achieved at a fiber volume fraction of 2 % was 210.9 MPa, which is 38 % higher than that of the plain UHPC without fibers. The compressive strength of UHPFRC with SS fibers exhibited an increase with the rise in fiber volume fraction up to 2 %, after which it slightly decreased. Yang et al. (2021), Meng et al. (2022), and Yoo et al. (2014b) consistently reported an increase in compressive strength of UHPC by incorporating steel fibers and by

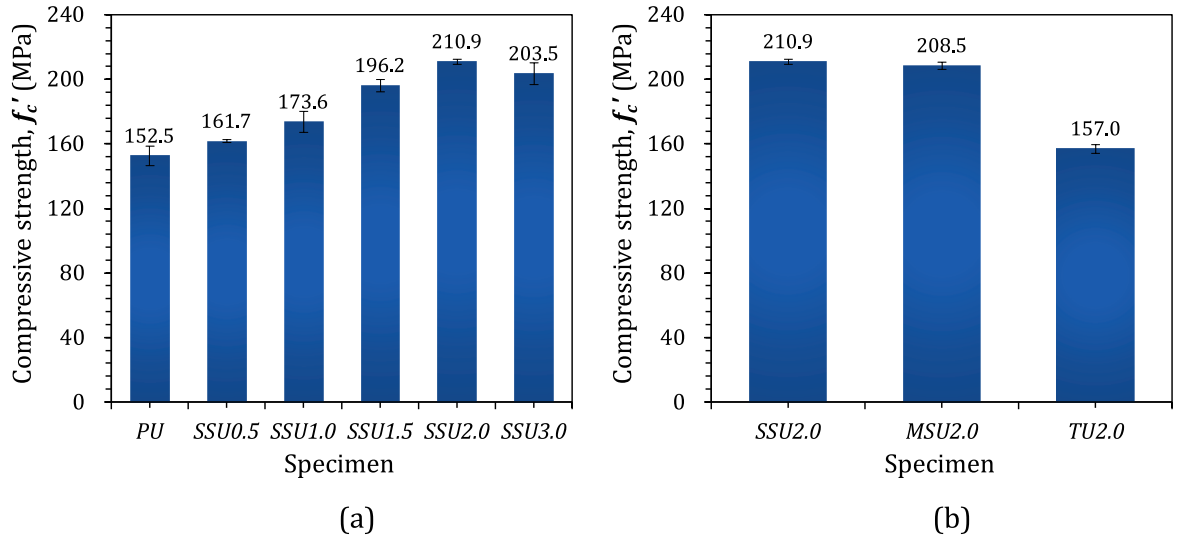

Fig. 4. Summary of compressive strengths of UHPC and UHPFRC: (a) effect of SS fiber volume content and (b) effect of steel fiber type.

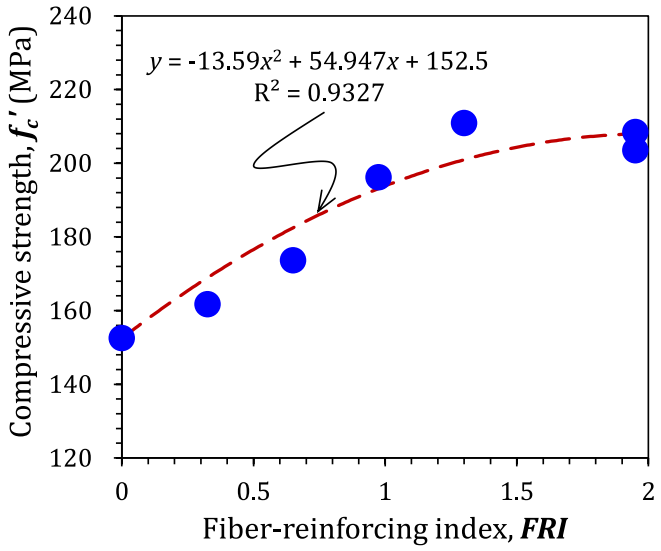

Fig. 5. Correlation between the compressive strength and FRI of SFRC.

increasing the volume fraction up to a certain dosage. This is because the incorporated steel fibers inhibit the propagation and widening of microcracks (Yoo and Yang, 2018). However, a higher fiber volume content also leads to an increase in air content (Soulioti et al., 2011) and, possibly, fiber balling, thus causing poor dispersion of the fibers. Soulioti et al. (2011) reported that the air content of fresh concrete initially decreased at a low fiber volume fraction of 0.5 % but continuously increased with an increase in volume fraction of fibers up to 1.5 %. Owing to the pros and cons of steel fibers, a slightly decreased compressive strength of 203.5 MPa was observed at the highest fiber volume fraction of 3 %.

Fig. 4b compares the effects of the fiber aspect ratio and shape on the compressive strength of the UHPFRC at an identical volume fraction of 2 %. Similar compressive strengths were obtained for the cases of SS and MS fibers; however, noticeably lower compressive strength of 157.0 MPa was observed in the case of TS fiber. This was possibly caused by the longer length (i.e., 30 mm) and angular shape of the cross-section, which might have deteriorated the degree of fiber dispersion.

Song and Hwan (Song and Hwang, 2004) predicted the compressive strength of high-strength concrete containing steel fibers based on a quadratic function of the fiber volume fraction. In this study, fiber aspect ratios of 65 and 97.5 were adopted to predict the compressive strength of UHPFRC with straight steel fibers based on the FRI, which is a product of the fiber volume fraction and aspect ratio, instead of the fiber volume fraction. The proposed quadric function is as follows.

$$f'_{cf} = f'_c + aV_f\left(\frac{l_f}{d_f}\right) + b\left[V_f\left(\frac{l_f}{d_f}\right)\right]^2, \quad (1)$$

where f'_{cf} is the compressive strength of the UHPFRC; f'_c is the compressive strength of the UHPC without fibers; V_f is the fiber volume fraction; l_f/d_f is the fiber aspect ratio; and a and b are regression coefficients.

Based on nonlinear regression analysis, the coefficients were found to be $a = 54.95$ and $b = -13.59$. In Fig. 5, the compressive strength of the UHPFRC was well predicted by Eq. (1) with a high coefficient of determination (R^2) of 0.9327. This implies that the compressive strength

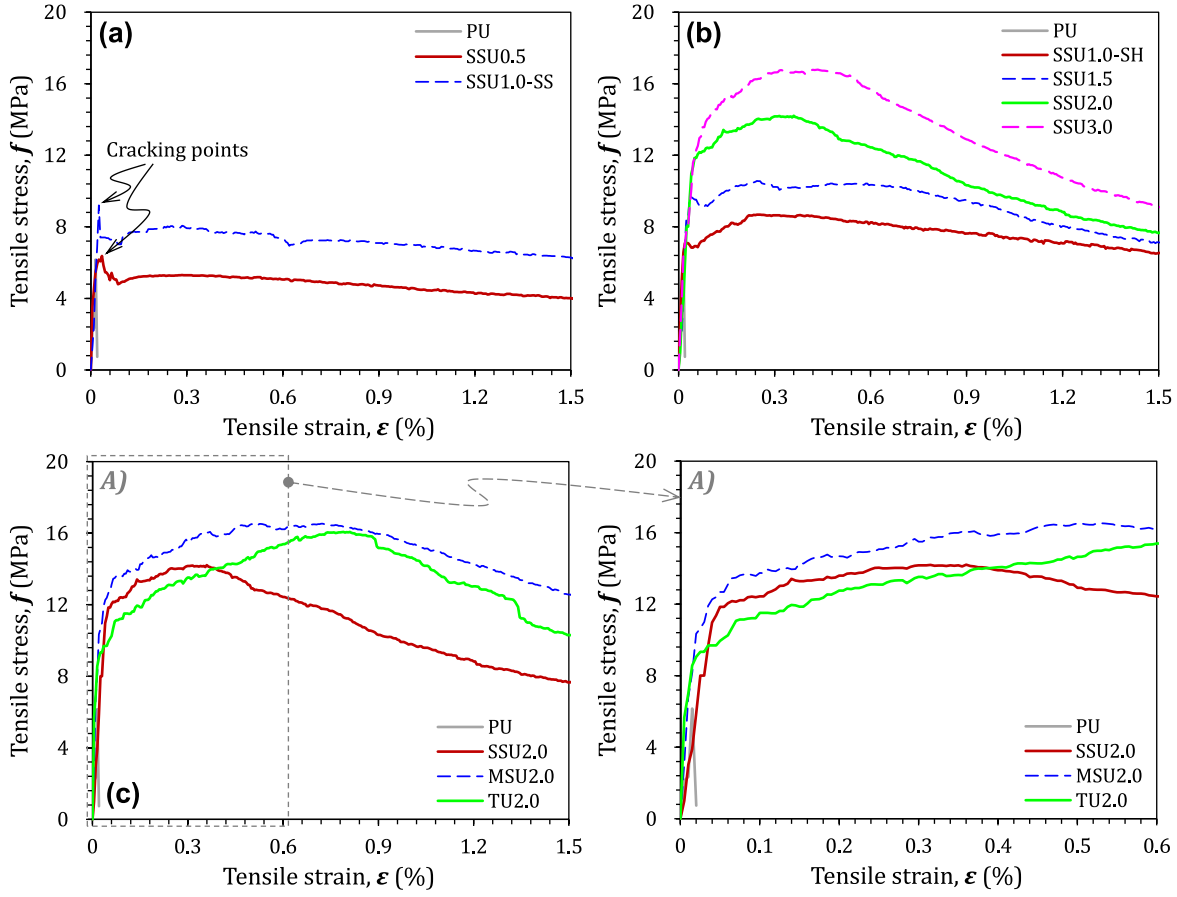

Fig. 6. Comparative tensile stress versus strain curves of UHPC and UHPFRC: (a) strain-softening UHPFRC, (b) strain-hardening UHPFRC, and (c) effect of steel fiber type [Note: *A)*: initial tensile behaviors].

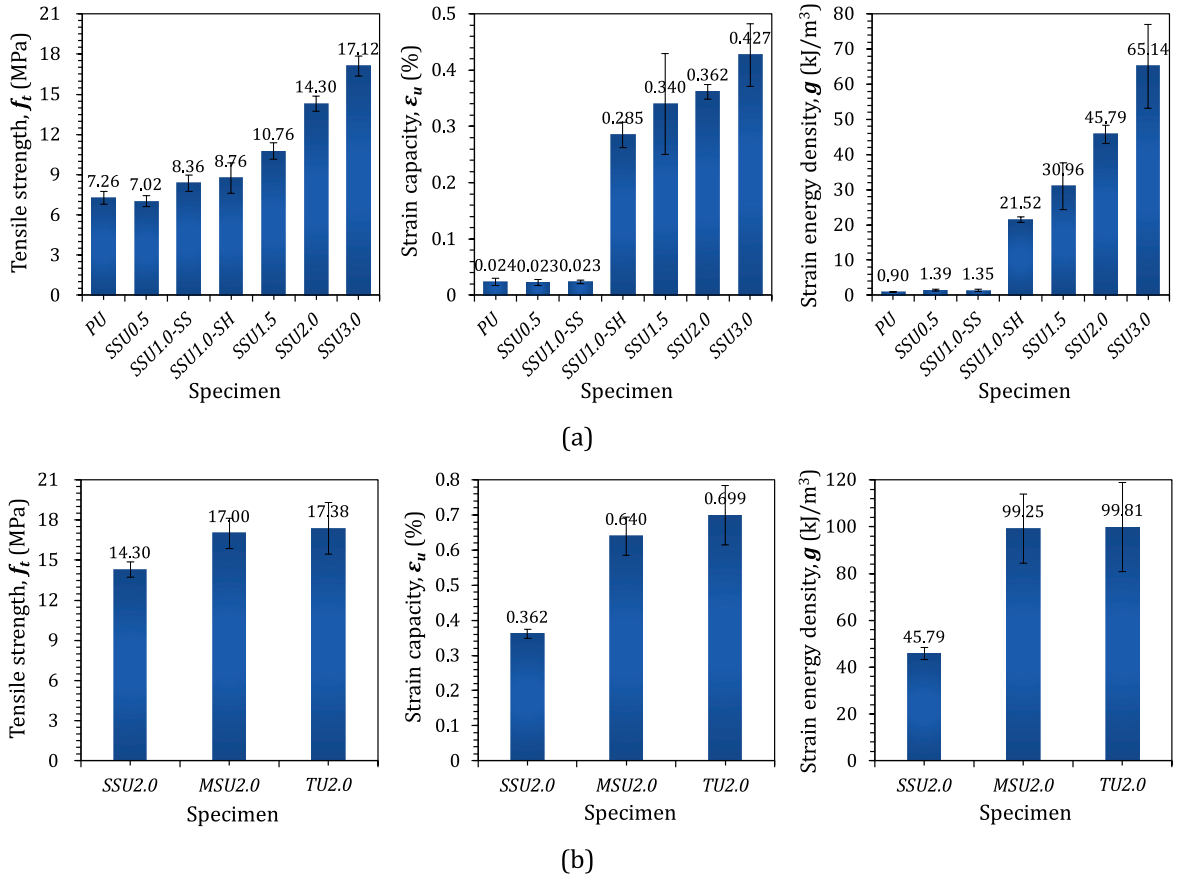

Fig. 7. Summary of tensile parameters of UHPC and UHPFRC: (a) effect of SS fiber content and (b) effect of fiber type at 2 vol%.

of UHPFRC is influenced by the FRI.

4.1.2. Direct tensile response

Fig. 6 shows the average tensile stress and strain curves of UHPC and UHPFRC. Very brittle tensile behavior was detected in the plain UHPC because of its ultrahigh strength and the absence of fibers. Linear elastic behavior was observed up to the peak strength, immediately after which, the stress dropped to almost zero. The brittle nature of the UHPC changed to a ductile nature by including steel fibers owing to their crack-bridging effect. At a low fiber volume fraction of 0.5 %, similar tensile strengths were obtained for the UHPC and UHPFRC (approximately 7 MPa); however, the post-peak tensile stress gradually decreased by bridging fibers at the crack surface. The maximum tensile strength of the SS0.5 specimen was observed at the initial cracking point; therefore, it can be categorized as a strain-softening material. According to a previous study by Meng et al. (2022), 0.5 % SS fibers resulted in a deflection-softening behavior under flexural conditions. When the fiber volume fraction increased from 0.5 % to 1.0 %, both strain-softening and strain-hardening behaviors were detected. Three of the five specimens exhibited strain-softening behavior, whereas the remaining two exhibited strain-hardening behavior. Therefore, the tensile behaviors of the SSU1.0 specimen were separated into two different curves in Fig. 6a and b. Both cases provided similar tensile strength values of 8.36–8.76 MPa; however, the strain capacity was different by 10-fold. Thus, the SSU1.0 specimen is considered as a material that barely exhibits strain-hardening behavior in tension. Tensile strain-hardening characteristics were observed when the volume fraction of SS fibers was ≥1.5 %. Specimens SSU1.5, SSU2.0, and SSU3.0 can be considered as strain-hardening materials. By increasing the volume fraction of fibers, the post-cracking tensile strength of the UHPFRC increased, although the initial cracking strength changed only slightly. Yoo et al. (2017a) observed that the fiber volume content had minimal influence on the first cracking strength, as it was primarily influenced by the matrix strength rather than the effect of fiber bridging capability. However, the post-cracking strength was predominantly determined by the strength of fiber bridging (Yoo et al., 2017a; Huang et al., 2018; Lee et al., 2011), which increases with increasing fiber content (Yoo et al., 2017a; Huang et al., 2018). Important tensile parameters, such as the tensile strength (f_t), strain capacity (ε_u), and strain energy density (g-value), are summarized in Fig. 7. The tensile strength gradually increased with the fiber volume fraction, and the highest value of f_t (17.1 MPa) was found in the SSU3.0 specimen, approximately 2.4 times higher than that of the plain UHPC specimen. However, both the strain capacity and energy absorption capacity changed significantly at a V_f of 1.0 % because these parameters were significantly influenced by the strain-hardening or -softening behavior. In addition, a higher fiber content resulted in higher values of ε_u and g. Thus, the highest ε_u and g values, found to be 0.43 % and 65.1 kJ/m^3, were observed in the SSU3.0 specimen, and they were 17.8 and 72.6 times higher than those of the plain UHPC specimen, respectively. This suggests that the inclusion of steel fibers is more impactful in enhancing the deformability and energy absorption capacity of UHPC rather than improving its tensile strength.

The effects of the fiber aspect ratio and shape on the tensile behavior of the UHPFRC at the same V_f of 2 % are shown in Fig. 6c. The use of MS and TS fibers resulted in an obvious improvement in the tensile performance compared with using only SS fibers. Twist torque was applied as an additional bond component between the TS fiber and the UHPC matrix, which resulted in a much higher pullout resistance than that of the SS fiber (Wille and Naaman, 2012). The MS fiber was longer than the SS fiber with an identical diameter of 0.2 mm. Although the number of MS fibers was lower than that of the SS fibers when UHPFRC was mixed, the actual number of fibers located at the localized crack surface was

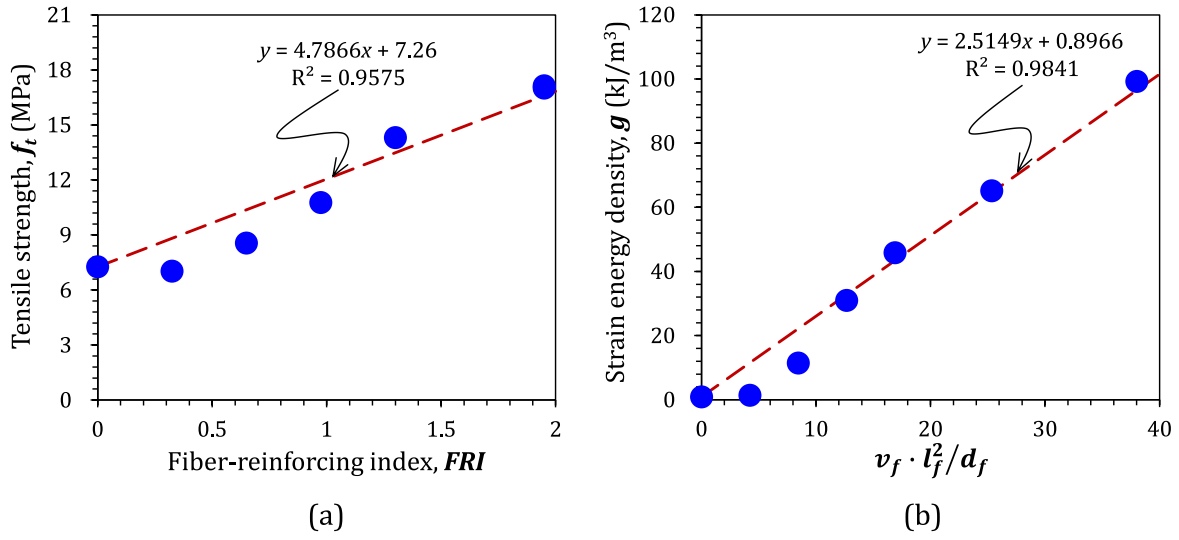

Fig. 8. Relations of (a) tensile strength and FRI and (b) strain energy density and FRI × l_f.

similar owing to the higher possibility of fiber detection at the crack surface for the former (Yoo et al., 2014a). As the MS fibers had a higher bonding area with the UHPC matrix, they exhibited a better bridging capability than the SS fibers. As shown in Fig. 7b, the TS fiber specimen exhibited the highest tensile strength of 17.4 MPa, followed by the MS and SS fiber specimens. Further, approximately 20 % higher f_t value was achieved using the MS and TS fibers, compared with the SS fibers. The strain and energy absorption capacities were also improved using the MS and TS fibers instead of the SS fibers, and the increase rates were higher than that of the f_t value. For example, the values of ε_u and g increased by 93 % and 118 %, respectively, compared with SS fibers when TS fibers were used. Thus, high strain energy densities of 99.2 and 99.8 kJ/m^3 were achieved in the cases of MS and TS fiber specimens, respectively. Although the SSU3.0 specimen had a higher V_f than those of the MSU2.0 and TU2.0 specimens, the latter resulted in a better energy absorption capacity. According to Wille et al. (2014), most UHPFRC reported in the

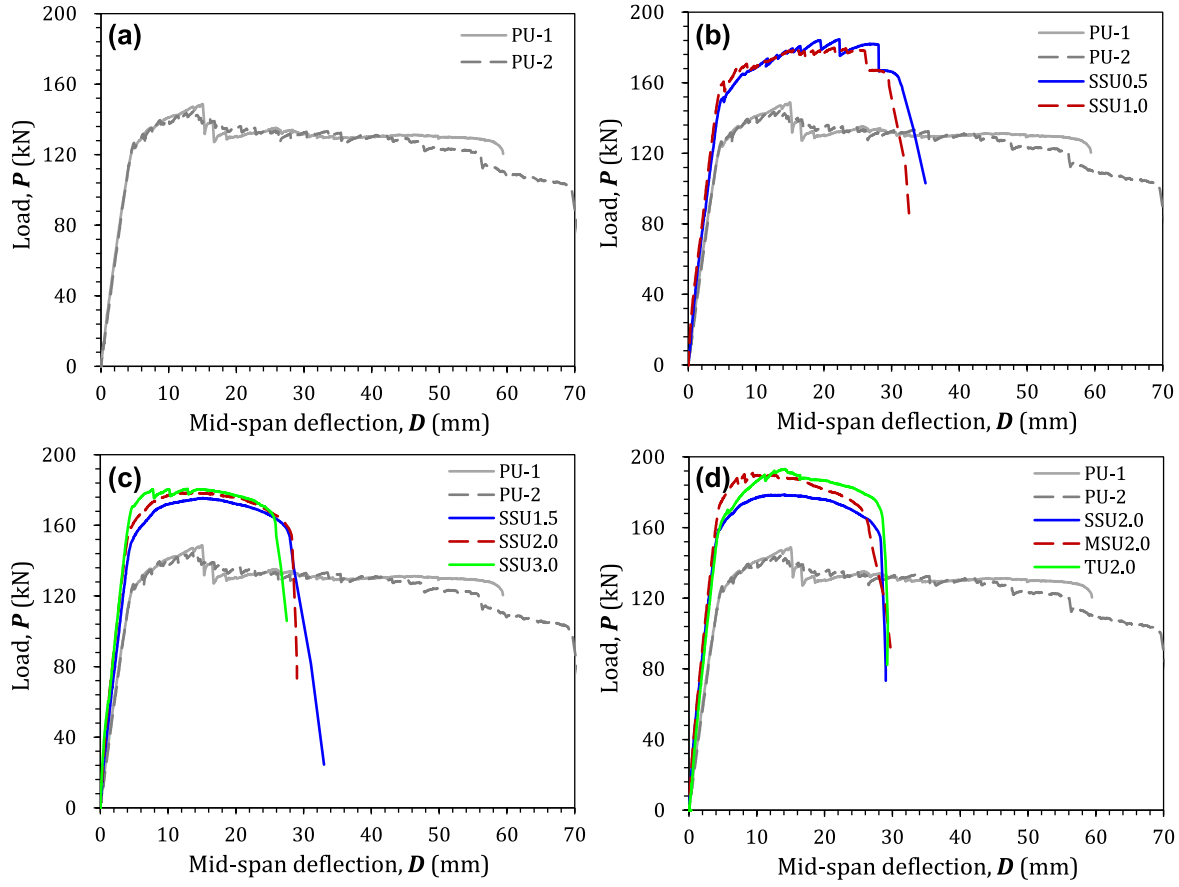

Fig. 9. Summary of load versus mid-span deflection curves: (a) plain UHPC beams (PU), (b) strain-softening UHPFRC beams (SSU-0.5 % and 1.0 %), (c) strain-hardening UHPFRC beams (SSU-1.5 %, 2.0 %, and 3.0 %), and (d) effect of steel fiber type at v_f of 2.0 % (SSU-2.0 %, MSU-2.0 %, and TU-2.0 %).

Fig. 10. Pictures of failed reinforced UHPC and UHPFRC beams.

literature have g-values of 55–94 kJ/m^3. Thus, the UHPFRCs with MS and TS fibers tested in this study are considered to be among the best energy-absorbent UHPFRC materials currently available.

4.1.3. Regression analysis on tensile parameters

The relationships between the tensile strength and FRI, and the strain energy density and quantity $V_f(l_f^2/d_f)$ are shown in Fig. 8. The post-cracking tensile strength has a linear relationship with the FRI and is expressed as: $\sigma_{pc} = \Lambda\tau_{eq}V_f(l_f/d_f)$, where Λ is the product of several coefficients involving the expected pullout length, orientation efficiency factor, group reduction factor, and snubbing coefficient; and τ_{eq} is the equivalent bond strength (Naaman, 2003). In addition, the pull-out surface energy is a good estimate of the fracture energy under tension and is expressed as a function of the quantity $V_f(l_f^2/d_f)$ (Pyo et al., 2015). Therefore, the values of f_t and g were fitted to the following equations.

$$f_t = f_{tp} + \alpha V_f\left(\frac{l_f}{d_f}\right), \tag{2}$$

$$g = g_p + \beta V_f\left(\frac{l_f^2}{d_f}\right), \tag{3}$$

where f_t and g are the tensile strength and strain energy density of UHPFRC, respectively; f_{tp} and g_p are the tensile strength and strain energy density of UHPC without fibers, respectively; $V_f(l_f/d_f)$ is the FRI; and α and β are regression coefficients.

The regression coefficients and R^2 values are shown in Fig. 8. The tensile strength and strain energy density fit well with Eqs. (2) and (3) with high R^2 values of 0.9575 and 0.9840, respectively. This verifies that the quantities $V_f(l_f/d_f)$ and $V_f(l_f^2/d_f)$ are the dominant factors affecting

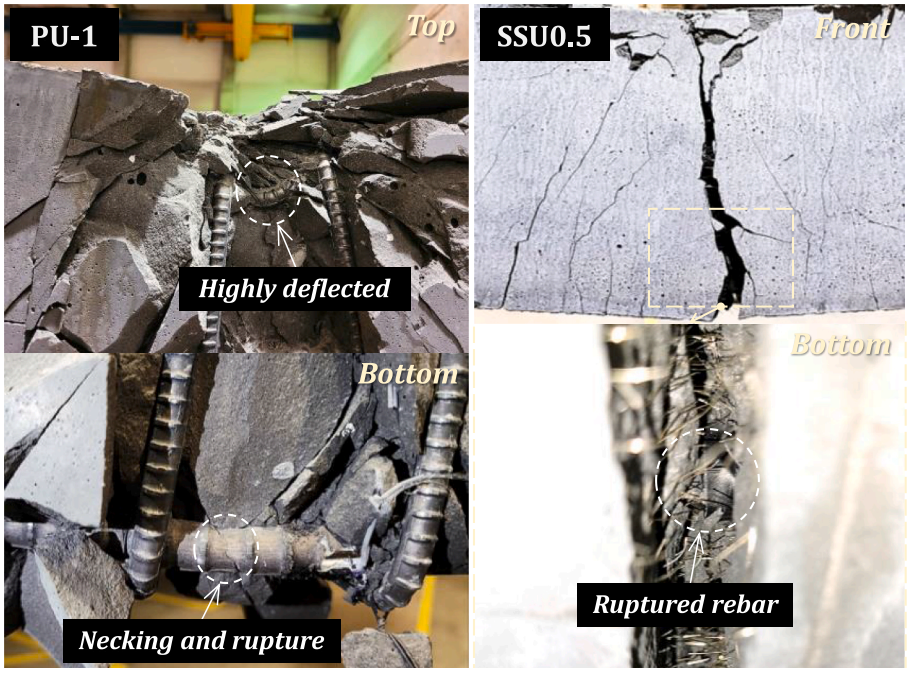

Fig. 11. Typical pictures of ruptured and highly deflected steel rebars.

Table 4
Summary of flexural test results of R–UHPC and R–UHPFRC beams.

Designation	FRI	At yield	At peak		At ultimate	Ductility index	
		Deflection, Δ_y [mm]	Load, P_p [kN]	Deflection, Δ_p [mm]	Deflection, Δ_u [mm]	μ_p	μ_u
PU-1	0.00	5.38	148.9	15.04	59.62	2.79	11.07
PU-2	0.00	5.23	144.8	13.71	69.62	2.62	13.30
SSU0.5	0.33	5.53	184.7	22.30	31.74	4.03	5.74
SSU1.0	0.65	4.99	179.9	21.56	29.66	4.32	5.94
SSU1.5	0.98	5.01	175.7	15.11	28.00	3.02	5.59
SSU2.0	1.30	4.49	178.7	13.86	28.33	3.09	6.31
SSU3.0	1.95	4.42	180.8	12.87	25.97	2.91	5.88
MSU2.0	1.95	4.54	191.1	9.42	27.22	2.07	5.99
TU2.0	2.00	5.16	193.3	14.19	29.00	2.75	5.62

[Note] FRI = fiber-reinforcing index, μ_p = ductility index at the peak, and μ_u = ductility index at the ultimate.

the tensile strength and *g*-value of UHPFRC.

4.2. Flexural behaviors of R–UHPC and R–UHPFRC beams

4.2.1. General behavior

The load versus mid-span deflection curves of the R–UHPC beam are shown in Fig. 9a. Initially, an almost linear increase in load was observed until the longitudinal steel rebar reached its yield strength. Subsequently, the flexural stiffness substantially decreased owing to the yielding of the steel rebar; however, the load-carrying capacity increased up to the maximum point owing to the strain-hardening behavior of the steel rebar under tension. The maximum flexural strength was obtained at a mid-span deflection of about 15 mm, after which the load decreased owing to the spalling and crushing of the UHPC in the compressive zone and the formation of cracks parallel to the top steel rebars generated from the loading point. The R–UHPC beams finally failed owing to the rupture of the longitudinal steel rebars at a deflection of approximately 59.6–69.6 mm. As shown in Fig. 10a, multiple flexural cracks formed near the mid-span of the R–UHPC beam because the tensile stress was transferred to the surrounding concrete through the bond between the steel rebars and concrete. The widths of multiple flexural cracks were sufficiently large to be detected by the naked eye. This implies that the deformation of the longitudinal steel rebars can be distributed through the zone of multiple flexural cracks, thus leading to a much larger ultimate deflection of the beam with rebar rupture. In Fig. 11, necking and rupture of the longitudinal steel rebar in the R–UHPC beam were clearly detected. Owing to its ultrahigh strength and absence of coarse aggregates, UHPC cracked into pieces with very sharp shapes. Spalling and parallel cracks began to form in the UHPC at the top of the beam near the peak load point (Fig. 10a). Owing to the UHPC spalling, the top rebar was even deflected at the end of the flexural test (Fig. 11).

Fig. 9b shows the comparative flexural behaviors of R–UHPC and R–UHPFRC beams with strain-softening characteristics under tension. The inclusion of steel fibers allowed for the absorption of a portion of the tensile stress at the surfaces of cracks. Consequently, higher post-cracking flexural stiffness and flexural strength were achieved in the SSU0.5 and SSU1.0 specimens that is coherent to the findings of Ashour and Wafa (1993) that steel fibers enhance the post-cracking stiffness and flexural rigidity of reinforced concrete beams, resulting in improved deflection control. Further, the deflections of the R–UHPFRC beams were lower than those of the R–UHPC beams, given the same loading levels. The post-yielding stiffness was not significantly affected by the relatively small dosages of SS fibers; however, the load-carrying capacity continued to increase beyond the deflection capacity of the R–UHPC beams. This is because the steel fibers prevented spalling of the matrix and top crack formation (Fig. 10b and c). The repetitive load drop and increase detected in the SSU0.5 and SSU1.0 specimens were caused by the slippage of the longitudinal steel rebar from the UHPFRC along with a formation of multiple flexural cracks. Similar to the plain beam, specimens SSU0.5 and SSU1.0 finally failed owing to the sudden load drop, which was attributed to the rupture of the longitudinal steel rebars; however, the ultimate deflection capacities were much lower than those of the R–UHPC beam. This is consistent with the findings of Yoo and Yoon (2015), and this can be attributed to the exceptional bond strength between the deformed steel rebar and UHPFRC, as well as the phenomenon of crack localization. The steel fibers inhibit the formation and widening of cracks such that the deformation of steel rebars is localized, thus leading to their premature rupture. As shown in Fig. 10b and c, multiple flexural and flexural-shear cracks were formed in the SSU0.5 and SSU1.0 beams; however, most of them were excessively tiny microcracks, which is inconsistent with the crack patterns of the R–UHPC beams. In accordance with Monte et al. (2024), UHPFRC exhibited a faster and more uniform self-healing process, attributed to the substantial presence of anhydrous particles and the formation of extremely narrow cracks resulting from multiple cracking. The tiny microcracks formed in the R–UHPFRC beams are expected to contribute to enhanced durability, thanks to their crack self-healing characteristics. One of the multiple cracks was localized, and the longitudinal steel rebar was then ruptured at the localized crack surface (Fig. 11). By increasing a volume fraction of steel fibers from 0.5 % to 1.0 %, the ultimate deflection, corresponding to the point of rebar rupture, decreased from 31.7 to 29.7 mm.

Fig. 9c shows the flexural behaviors of the R–UHPFRC beams that exhibited strain-hardening behavior (SSU1.5, SSU2.0, and SSU3.0) compared with those of the R–UHPC beams. In contrast to the SSU0.5 and SSU1.0 beams, smooth post-yield load–deflection curves were obtained with a higher flexural stiffness. The maximum flexural load increased as the fiber volume fraction increased from 1.5 % to 3.0 %; however, as the fiber volume fraction increased, the deflection capacity at the peak load and ultimate deflection decreased. For example, the ultimate deflection decreased from 28.0 to 26.0 mm when V_f increased from 1.5 % to 3.0 %. The number of flexural cracks in the R–UHPFRC beams decreased noticeably when the V_f was 1.5 % or higher, and most of the longitudinal deformation was localized to one or two cracks (Fig. 10d–f). The tensile strain-hardening characteristics of the UHPFRC negatively affected the cracking behavior and stress redistribution of the R–UHPC and R–UHPFRC beams. This might be due to the deterioration of fiber orientation owing to fiber interference. Meng et al. (2022) reported that the fiber orientation factor (η_θ) of UHPFRC decreased from 0.80 to 0.61 when the V_f increased from 0.5 % to 2.0 %. The lower η_θ value implies that more fibers are inclined to the longitudinal direction, thus resulting in a decreased number of fibers detected at the surface of localized crack (Yoo et al., 2015b). The further increase in tensile stress, transferred from the steel rebars and fibers to the surrounding UHPFRC, was limited to the weakest part (localized crack) owing to the deteriorated fiber orientation. Thus, it became more difficult to generate multiple cracks because the remaining parts attained higher tensile strength through the existence of more fibers. Specimens SSU1.5, SSU2.0, and

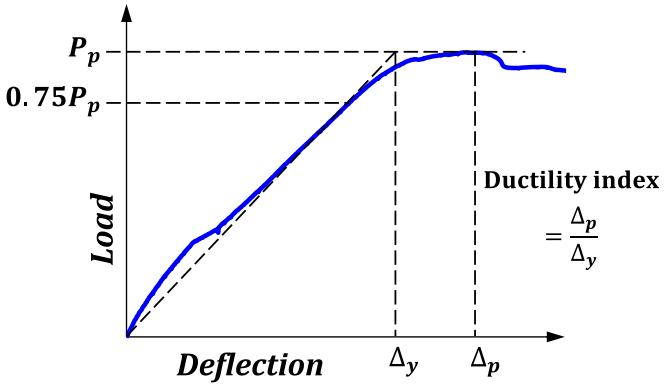

Fig. 12. Schematic description of yield deflection (Δ_y) based on reduced stiffness equivalent elasto-plastic yield (Park, 1988).

SSU3.0, all failed by the rupture of steel rebars, and because of the limited distribution of rebar deformation, they exhibited rebar rupture earlier than the R–UHPC and strain-softening R–UHPFRC beams.

For a fixed V_f of 2 %, the fiber aspect ratio and shape also influenced the flexural capacity of the R–UHPFRC beams, as shown in Fig. 9d. The use of MS and TS fibers was more effective in increasing the flexural strength of R–UHPFRC beams because their higher aspect ratio and untwisting torque improved the post-cracking tensile properties. This result is consistent with the findings of Yoo and Yoon (2015). For instance, the maximum loads of the MSU2.0 and TU2.0 specimens were 191.1 and 193.3 kN, respectively, approximately 6.9–8.2 % higher than that of the SSU2.0 specimen (Table 4). However, no trends were observed in the deflection capacity or ultimate deflection. The deflection capacity and ultimate deflection of the TU2.0 specimen were 14.2 and 29.0 mm, respectively, larger than those of the SSU2.0 specimen; however, the MSU2.0 specimen resulted in lower values of 9.4 and 27.2 mm, respectively. As shown in Fig. 10g and h, the MSU2.0 and TU2.0 specimens exhibited localized flexural cracks and finally failed owing to longitudinal steel rebar ruptures.

4.2.2. Ductility

Yield deflection is defined based on an equivalent elastoplastic system with decreased stiffness (Park, 1988), as shown in Fig. 12. Defining the yield point from the flexural load–deflection curves is challenging because of the material nonlinear behavior and the formation of plastic hinges in different parts of the beam at different load levels (Park, 1988). Thus, herein, a secant stiffness of 75 % of the peak load was used owing to the crack formation near the end of the elastic range. Subsequently, the ductility indices were calculated using Eqs. (4) and (5), based on the deflections corresponding to the peak, ultimate, and yield states (Shin et al., 1989).

$$\mu_p = \frac{\Delta_p}{\Delta_y}, \tag{4}$$

$$\mu_u = \frac{\Delta_u}{\Delta_y}, \tag{5}$$

where Δ_p is the peak load deflection; Δ_y is the steel-bar yielding deflection; and Δ_u is the ultimate deflection.

The ductility indices are given in Table 4 and Fig. 13. The average ductility indices at the peak and ultimate states of the plain UHPC beams were 2.71 and 12.19, respectively. The steel fiber volume content significantly influenced the ductility indices. The ductility index at the peak, μ_p, of the R–UHPC beams first increased by adding steel fibers up to V_f of 1 %, and subsequently, it decreased to have similar values to that of the R–UHPC beams. This indicates that only small amounts of steel fibers exhibiting strain-softening characteristics are effective in increasing the peak ductility index of R–UHPC beams. This is similar to the results obtained by Saqif et al. (2022), who reported that an increase in the material ductility of UHPFRC does not necessarily translate into an increase in the structural ductility of lightly reinforced UHPFRC beams. Although most of the R–UHPFRC beams that exhibited strain hardening under tension also exhibited slightly higher peak ductility indices, the differences between the peak ductility indices of the R–UHPC and R–UHPFRC beams were insignificant.

However, regardless of the fiber volume fraction and tensile characteristics (strain-softening or -hardening), the ultimate ductility index, μ_u, of the R–UHPC beams decreased significantly owing to the addition of steel fibers. The μ_u value decreased from 12.19 for the R–UHPC beams to 5.59–6.31 for R–UHPFRC beams, which corresponds to approximately 45.9–51.8 % reduction. In addition, among the R–UHPFRC beams, the SSU2.0 specimen exhibited the highest μ_u value of 6.31, and it generally increased and decreased based on the fiber volume fraction of 2 %. Similarly, Yang et al. (2020) reported that the ductility index of R–UHPFRC beams increased with an increase in V_f of steel fibers from 1.0 % to 1.5 % and decreased at a higher fiber V_f of 2 %. The presence of steel fibers is a predominant factor affecting the ductility of R–UHPC beams at low reinforcement ratios (Yang et al., 2020). Saqif et al. (2022) also noted that the deflection ductility index of R–UHPFRC beams is influenced by the strain-hardening ratio ($\varepsilon_t/\varepsilon_{cr}$). Structural ductility increased with the $\varepsilon_t/\varepsilon_{cr}$ ratio up to 20 and then decreased afterward.

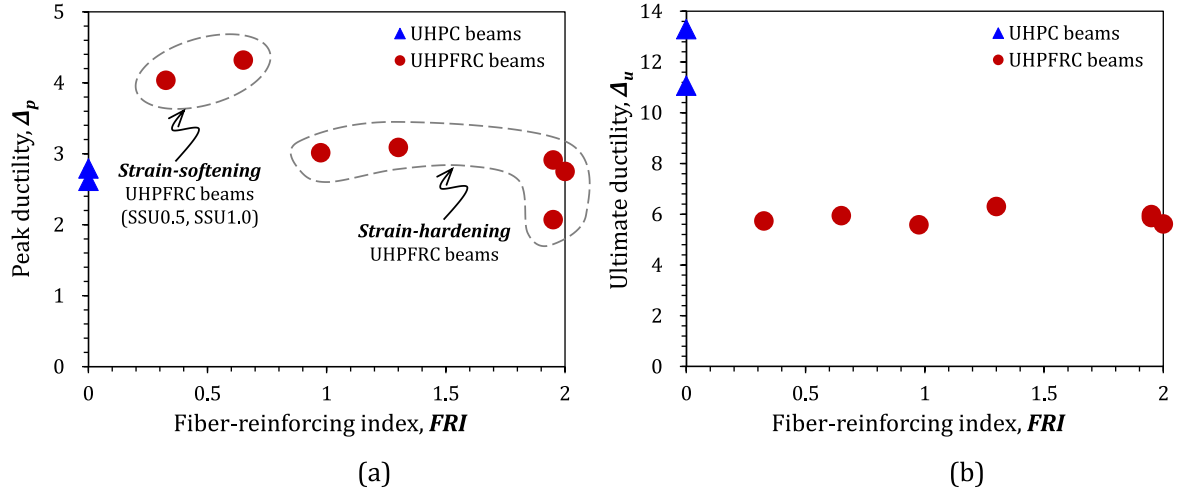

Fig. 13. Effect of FRI on the (a) peak ductility and (b) ultimate ductility.

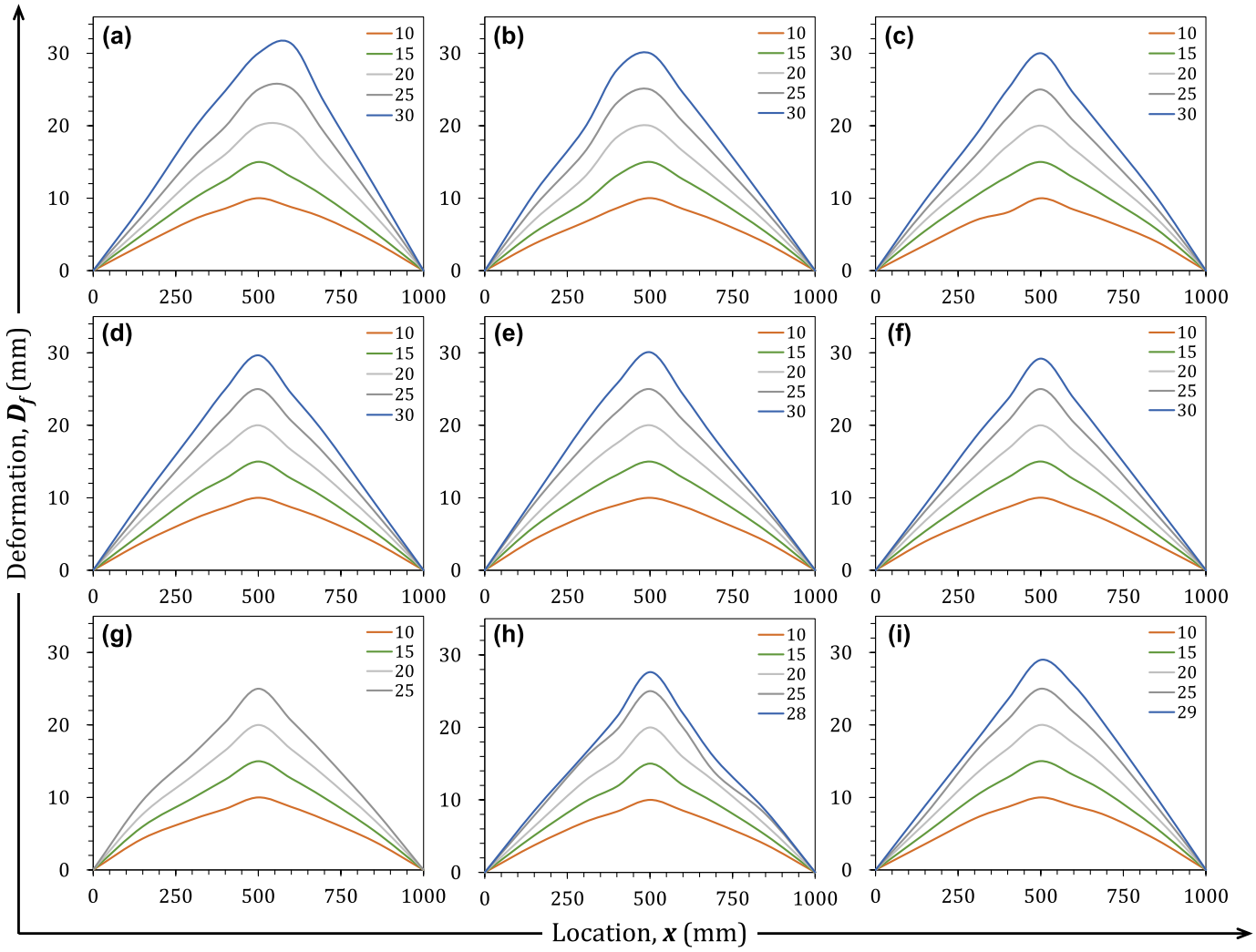

Fig. 14. Summary of deformation shapes of reinforced UHPC and UHPFRC beams: (a) PU-1, (b) PU-2, (c) SSU0.5, (d) SSU1.0, (e) SSU1.5, (f) SSU2.0, (g) SSU3.0, and (h) MSU2.0, (i) TU2.0.

This indicates that better strain-hardening behavior of UHPFRC does not ensure better structural ductility of R–UHPFRC beams. A potential reason for this is the crack localization phenomenon of UHPFRC, which results in the concentration of inelastic deformation in few large cracks. Espion (1994) reported that the inelastic deformation in FRC beams is concentrated at the ultimate stage in one large crack, whereas it is more evenly distributed in concrete beams without fibers. The excellent bridging capabilities of the high volume of steel fibers at the crack surfaces prohibit the formation of more flexural cracks, which can be distributed throughout the beams, thus leading to concentrated deformation in the longitudinal steel rebars. Ashour (2000), Yoo and Moon (2018), and Qiu et al. (2020) reported that the ultimate ductility index decreases with an increase in the reinforcement ratio of high-strength concrete (HSC) or UHPFRC beams. Steel fibers are also a type of reinforcement that withstand tensile stresses at the crack surface, such as in steel rebars; thus, the ultimate deflection ductility, μ_u, of R–UHPC beams decreases with the addition of steel fibers. Yoo and Moon (2018) reported a reduction in the ductility index of RC beams with low reinforcement ratios, ranging from 0.178 % to 0.406 %, upon the addition of hooked steel fibers up to a volume fraction of 1.0 %. By contrast, other researchers (Ashour and Wafa, 1993; Abbass et al., 2019; Oh, 1992) reported an increased ductility index of RC beams with the inclusion of steel fibers. In accordance with Ashour and Wafa (1993), the ductility index, μ_u, of reinforced HSC beams with a shear span-depth ratio of 4 was 1.538, and it increased to 3.378 by including 1.5 % (by volume) steel fibers. Abbass et al. (2019) reported that the ductility indices of both solid and hollow RC beams increased from 3.7 to 5.5 and from 4.2 to 5.9, respectively, by adding 1.5 vol % hooked steel fibers. In their study (Abbass et al., 2019), a steel fiber-reinforced concrete (SFRC) mixture with V_f of up to 1.5 % exhibited deflection-softening behavior. These discrepancies are caused by the susceptibility of the ductility index of RC beams to various factors, such as the fiber content, reinforcement ratio, material tensile characteristics, and crack patterns. However, in the case of R–UHPC beams, the addition of steel fibers decreased the ultimate deflection ductility, μ_u, regardless of the fiber volume content, as presented in this study and previous studies (Yoo and Yoon, 2015; Yang et al., 2020).

4.2.3. *Deformation shape*

Fig. 14 summarizes the deformation shapes of the R–UHPC and R–UHPFRC beams at mid-span deflections of 10–30 mm. All the UHPFRC beams exhibited symmetric deformation shapes, even beyond the maximum load point, up to 30 mm (Fig. 14c–i). However, the UHPC beam (PU-1) exhibited symmetric deformation shapes only up to 15 mm near the maximum load point and left-skewed deformation shapes thereafter (Fig. 14a). This is caused by the widening of multiple distributively-formed flexural cracks. The effect of the steel fibers on the deformation shape of the R–UHPC beams is shown in Fig. 15. As shown

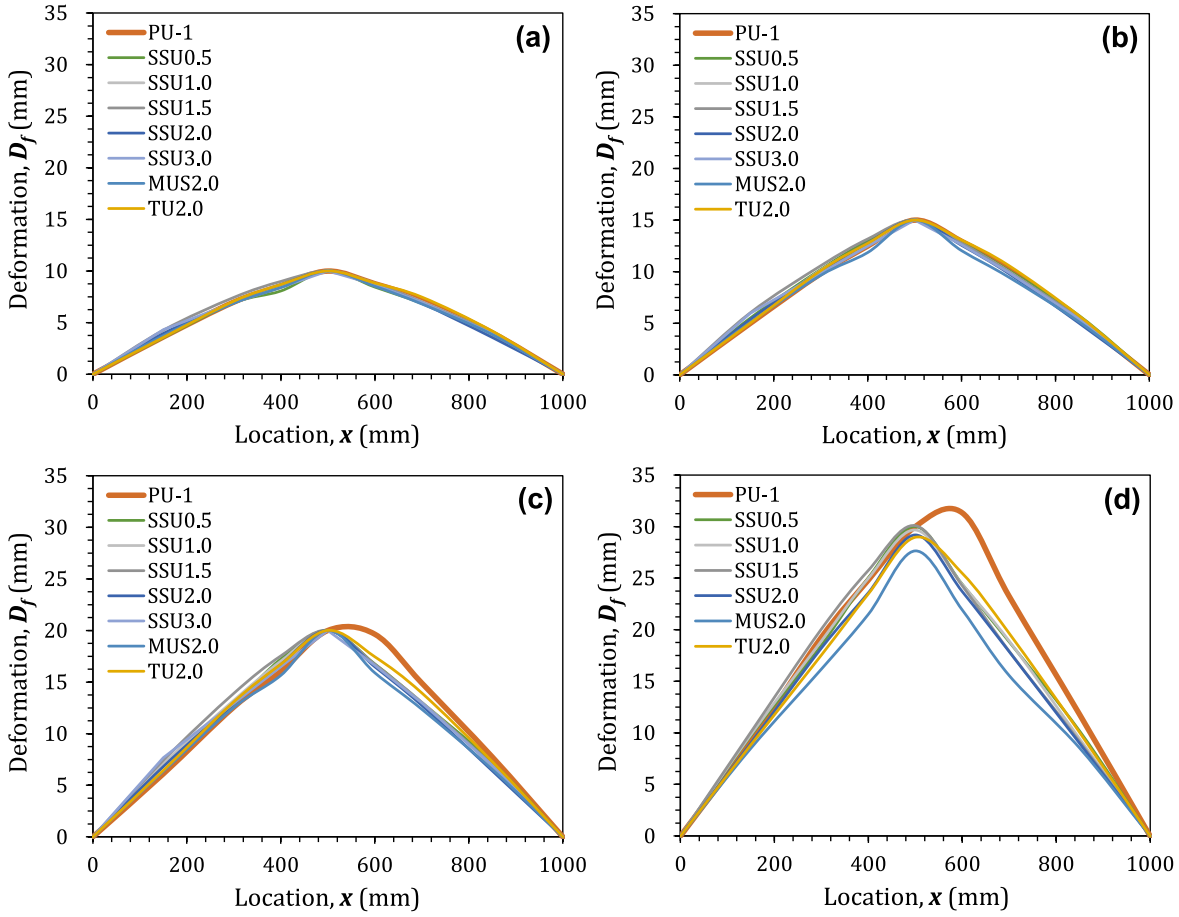

Fig. 15. –Comparative deformation shapes of reinforced UHPC and UHPFRC beams at deflection points of (a) 10 mm, (b) 15 mm, (c) 20 mm, and (d) 30 mm.

in Fig. 15a and b, the steel fibers had no clear effect on the deformation shape of the UHPC beams up to the maximum load point. However, beyond the maximum point, different deformation shapes were formed based on the presence of steel fibers (Fig. 15c and d). The UHPFRC beams exhibited sharper and more symmetric deflection shapes than the UHPC beams because the steel fibers bridged and controlled the widening of the cracks. As shown in Fig. 10, the UHPC beams developed multiple flexural cracks and caused an increase in their widths. The widened flexural cracks were distributed from the mid-span to the supports of the UHPC beams. However, the UHPFRC beams developed only few flexural cracks and limited the widening of most of them except single localized cracks. Therefore, the deformation shapes of the UHPC beams were gradual and skewed compared with those of the UHPFRC beams.

The deformation shapes of the UHPFRC beams were not significantly influenced by the steel fiber content, aspect ratio, or shape. In particular, although the strain-softening UHPFRCs (SSU0.5 and SSU1.0) developed multiple flexural cracks, in contrast to the strain-hardening UHPFRC, the deformation shapes of both the strain-softening and strain-hardening UHPFRC beams were similar as symmetry. Therefore, in conclusion, the inclusion of steel fibers affects the deformation shape of UHPC beams; however, the steel fiber properties have a minor impact on the deformation shape of UHPFRC beams.

4.3. FE analysis

A nonlinear FE analysis was conducted by considering the material models suggested from the experiments to predict the flexural behavior of the R–UHPFRC beams. Fig. 16 shows the FE mesh used in this analysis. The UHPFRC and steel rebars were modeled using the linear

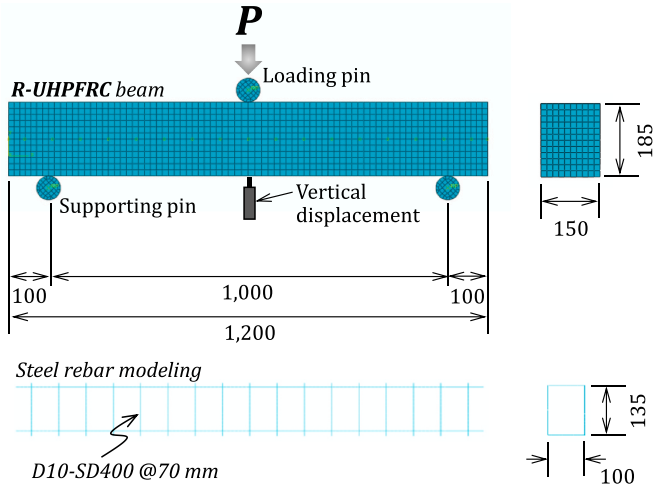

Fig. 16. Three-dimensional (3D) FE mesh and modeling of R–UHPFRC beam.

hexahedron element C3D8 and linear beam element B31, respectively, in the commercial finite element software ABAQUS (ABAQUS, 2021). The loading and supporting pins were modeled in accordance with the experimental setup. No interpenetrating displacement between the R–UHPFRC beam and the loading and supporting pins was allowed. ABAQUS provides several quasi-brittle material models, namely smeared cracking model, cracking model for concrete, and concrete damaged plasticity model. The concrete damaged plasticity model, which is generally used because it models simply the strain-hardening

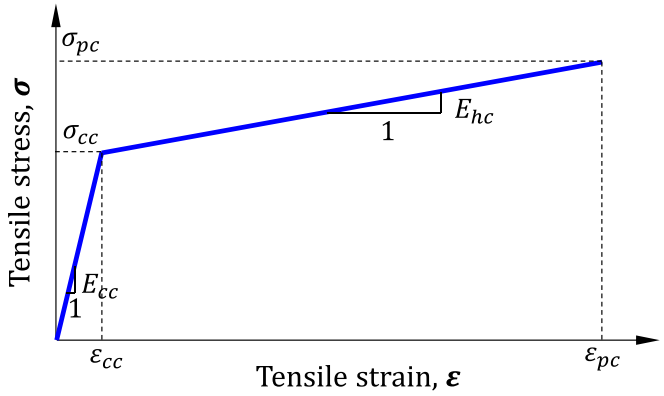

Fig. 17. Bilinear tensile modeling of UHPFRC used for FE analysis.

behavior, was adopted. The tensile behavior of the UHPFRC was modeled by considering its typical tensile properties, as reported by Wille et al. (2014). The tensile behavior was modeled as bilinear with two different zones: a strain-based elastic zone and strain-based hardening zone, as shown in Fig. 17, because the UHPFRC exhibited tensile strain-hardening behavior. Herein, σ_{cc} is the initial cracking strength, ε_{cc} is the cracking strain, E_{cc} is the elastic modulus, σ_{pc} is the post-cracking strength, and E_{hc} is the hardening modulus. These parameters were obtained from the tensile test results using a regression analysis based on the least-squares error method.

The flexural load and mid-span deflection curves of the reinforced UHPFRC beams obtained from the FE analysis at $K = 1$ are compared with the experimental results, as shown in Fig. 18. The initial flexural stiffness values of most of the R–UHPFRC beams obtained from the FE analysis were similar to those obtained experimentally. After the steel rebars yielded, the flexural stiffness decreased significantly, and hardening behaviors were observed in the FE analysis, similar to those in the experiments. In the case of the SS fiber-reinforced series, the load-carrying capacity and post-yield flexural stiffness, which increased with an increase in the fiber V_f, were precisely simulated through FE analysis. The FE analysis successfully simulated the increased maximum load and post-yield flexural stiffness of R–UHPFRC beams achieved due to the increase of the aspect ratio of SS fibers and incorporating TS fibers.

In Fig. 18d, the contour plot for the SSU1.5 specimen is representatively shown when the maximum load was applied. The distribution of the positive principal strain for the entire model is shown in Fig. 18d. As mentioned above, if a high volume of steel fibers is incorporated into UHPC, it exhibits a crack localization phenomenon owing to the superb bond strength between the deformed steel rebar and UHPFRC and the crack bridging capability. In the FE analysis, a similar trend was observed, thus indicating that the maximum principal strain was locally observed at the bottom center of the beam. The distribution of the von Mises stress of the steel rebars in Fig. 18d also indicates that the steel rebar yielded around the center of the beam. If a material model of UHPFRC that simulates crack propagation and element deletion is further developed using a user subroutine in ABAQUS, crack growth and clear crack localization can be simulated in the analysis.

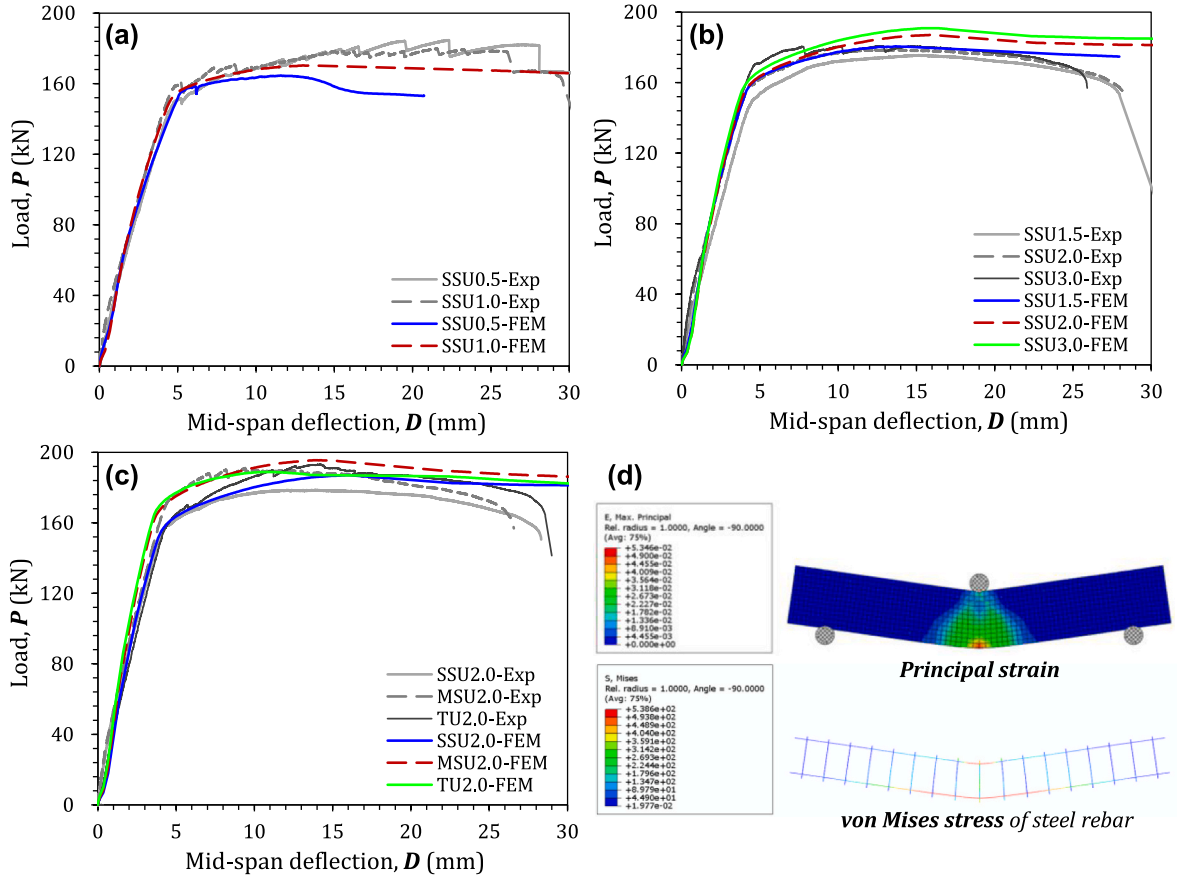

Fig. 18. Comparison of flexural load versus mid-span deflection curves between experiments and FE analysis: (a) strain-softening UHPFRC beams (SSU0.5 and SSU1.0), (b) strain-hardening UHPFRC beams (SSU1.5, SSU2.0, and SSU3.0), (c) effects of fiber aspect ratio and shape (SSU2.0, MSU2.0, and TU2.0), and (d) principal strain and von Mises stress contours of SSU1.5 (deformation scale factor = 5).

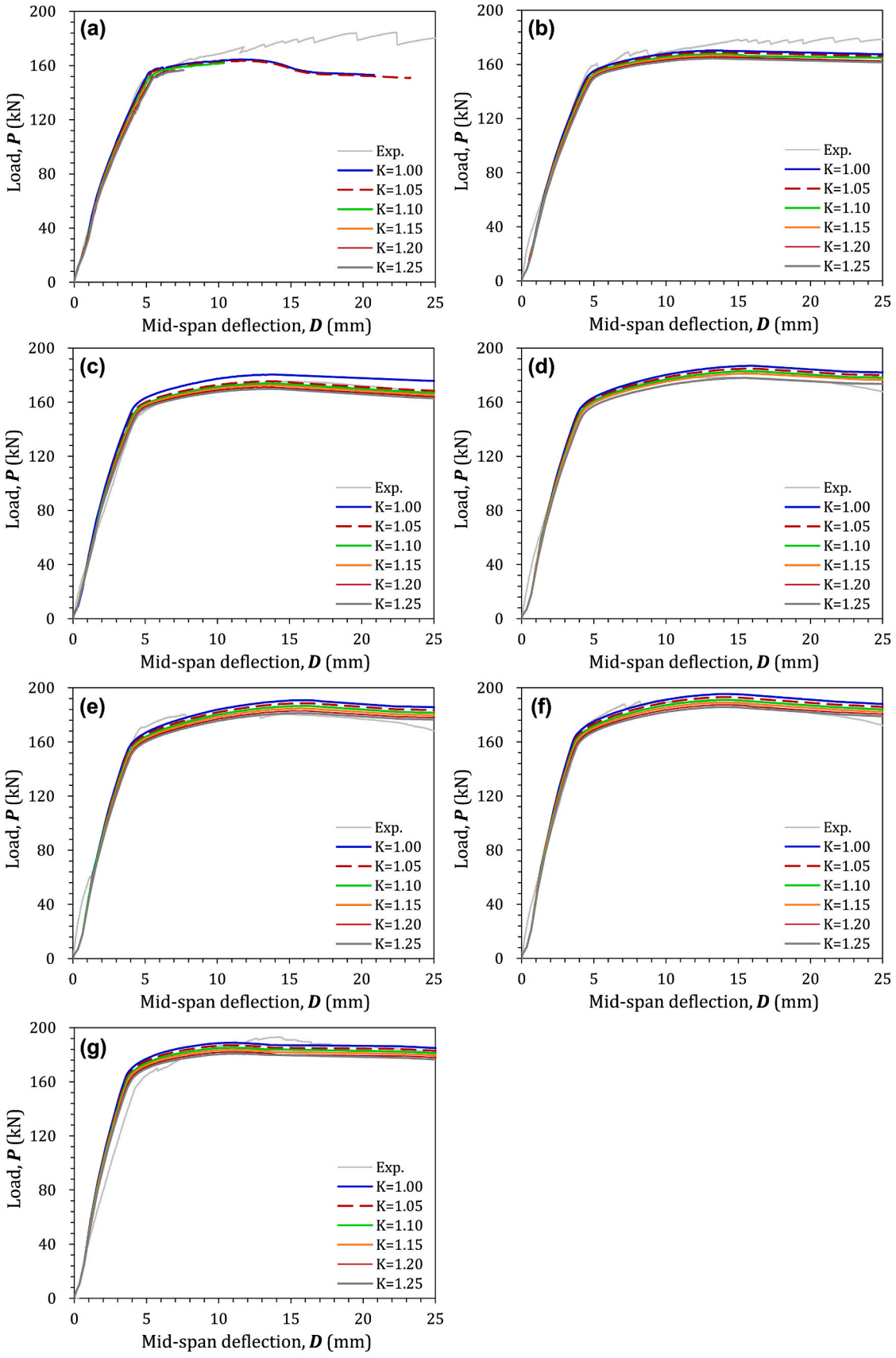

Fig. 19. Predictive load versus deflection curves according to the fiber orientation coefficient (*K*): (a) SSU0.5, (b) SSU1.0, (c) SSU1.5, (d) SSU2.0, (e) SSU3.0, (f) MSU2.0, and (g) TU2.0.

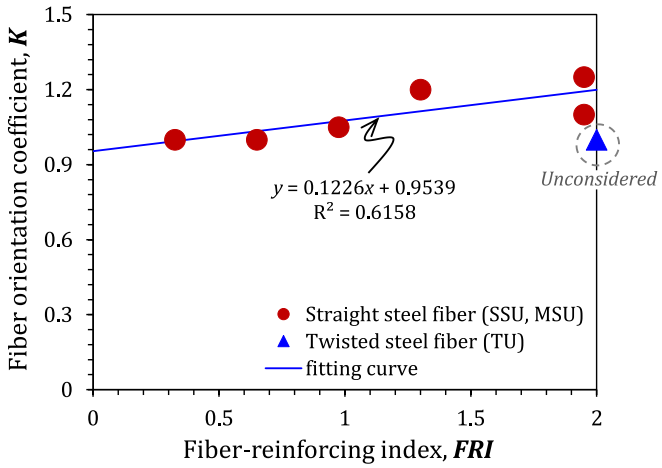

Fig. 20. Suggestion of fiber orientation coefficient (K) according to FRI.

4.4. Suggestion for the fiber orientation coefficient, K

An inverse analysis by varying the fiber orientation coefficient K was conducted to determine the appropriate coefficient according to the FRI. Based on the AFGC recommendations (AFGC, 2013), the tensile stresses were modified by considering the coefficient K. Subsequently, initial cracking and post-cracking tensile stresses were changed to σ_{cc}/K and σ_{pc}/K, respectively. The AFGC recommendations (AFGC, 2013) suggested $K = 1.25$ for all loading conditions other than local effects to consider the random fiber orientations. However, the degree of random fiber orientation is affected by parameters such as the fiber aspect ratio (Yoo et al., 2014a), shape, and volume fraction (Meng et al., 2022). Thus, the variation in the coefficient K according to the FRI need to be analyzed.

Six K values, ranging from 1.00 to 1.25, were considered. The coefficient K with the smallest difference between the maximum loads obtained from the analysis and experiments was selected as the appropriate value. Fig. 19 shows the flexural load and mid-span deflection curves obtained from the inverse analysis. As shown in Fig. 19, the flexural behavior of the reinforced UHPFRC beams was slightly changed by the coefficient K, and most of the FE analytical results were similar to those from the experiments.

Based on the results of the inverse analysis, the selected appropriate fiber orientation coefficient, K, is summarized in Fig. 20. As shown in the figure, the coefficient K can be simulated as a linear function of the FRI, as follows.

$$K = cV_f\left(\frac{l_f}{d_f}\right) + d, \tag{6}$$

where $V_f(l_f/d_f)$ is the FRI; and c and d are regression coefficients.

Due to the distinct bond mechanisms and cross-sectional shape of twisted steel fibers in comparison to straight steel fibers, the TU specimens were not taken into consideration when predicting the regression coefficients. Based on linear regression analysis, the values of c and d were found to be 0.1226 and 0.9539, respectively. As the TS fiber has different pullout mechanisms compared with the straight steel fiber, the result of the TU2.0 specimen was not considered to evaluate the coefficients c and d. The coefficient K was clearly influenced by the FRI and generally increased with increasing FRI. This is because fibers with a higher aspect ratio or higher volume fraction result in nonuniform dispersion by the interruption of the internal steel rebars. Thus, better predictions are obtained using Eq. (6), compared with the fixed coefficient K of 1.25, which changes according to the FRI.

5. Conclusions

This study investigated the effects of the steel fiber volume fraction, aspect ratio, and shape on the mechanical properties of UHPFRC and the structural behavior of R–UHPFRC beams under flexure. The mechanical strength was predicted using FRI, whereas the strain energy density was predicted based on the surface energy of the pull-out. Based on FE analysis, the fiber orientation coefficient, K, was suggested by considering the FRI. Based on the experimental and numerical results, the following conclusions were derived.

1) For the SS fiber, a fiber volume fraction of 1.0 % or less resulted in a strain-softening behavior under tension. The tensile strength and energy absorption capacity of UHPC were improved by incorporating SS fibers and increasing their content to 3.0 %. At an SS fiber volume fraction of 3.0 %, the tensile strength and strain energy density obtained (17.1 MPa and 65.1 kJ/m^3) were 2.4 and 72.6 times higher than those of plain UHPC, respectively.
2) The compressive and tensile strengths of UHPFRC were well predicted as a function of the FRI, whereas the strain energy density was predicted based on the quantity $V_f(l_f^2/d_f)$ with an R^2 higher than 0.98.
3) Given an identical fiber volume fraction of 2.0 %, the utilization of MS and TS fibers resulted in significantly improved tensile performance than that of SS fibers: more than twice the energy absorption capacity of approximately 100 kJ/m^3 was achieved. The flexural strength of the R–UHPFRC beam with SS fibers was also improved by using MS and TS fibers.
4) The flexural strength of the R–UHPC beam significantly increased by incorporating steel fibers and increasing the volume fraction up to 3.0 %, whereas the ultimate deflection decreased. The tensile strain-hardening characteristics of the UHPFRC deteriorated the cracking behavior and stress redistribution of the structural R–UHPC and R–UHPFRC beams.
5) Small amounts of SS fibers (V_f of $\leq$1.0 %) that exhibit strain-softening characteristics were effective to improve the peak ductility, μ_p, of R–UHPC beams. By contrast, the ultimate ductility, μ_u, of R–UHPC beams decreased significantly by 48.2–54.1 % through the incorporation of steel fibers owing to concentration of inelastic deformation in few large cracks.
6) Through nonlinear FE analysis, the flexural behavior of reinforced UHPFRC beams was accurately predicted. The fiber orientation coefficient K was not a fixed value but rather varied with the FRI. Thus, an appropriate coefficient K was suggested as a linear function of the FRI based on inverse analysis.

CRediT authorship contribution statement

Doo-Yeol Yoo: Conceptualization, Formal analysis, Investigation, Writing – original draft. **Salman Soleimani-Dashtaki:** Investigation, Methodology. **Taekgeun Oh:** Formal analysis, Investigation. **Booki Chun:** Data curation, Resources. **Nemkumar Banthia:** Supervision, Writing – review & editing. **Seung-Jung Lee:** Data curation, Formal analysis, Funding acquisition, Writing – original draft. **Young-Soo Yoon:** Supervision, Writing – review & editing.

Declaration of competing interest

The authors declare that they have no known competing financial interests or personal relationships that could have appeared to influence the work reported in this paper.

Data availability

The data that has been used is confidential.

Acknowledgements

This work was supported by the National Research Foundation of Korea (NRF) grant funded by the Korea government (MSIT) (No.2019R1C1C1008190). The structural experimental program was conducted at the University of British Columbia in Canada, and we would like to extend special thanks to Tyler Donovan and Sahar Jafar-Beglou for their invaluable assistance.

References

ABAQUS, 2021. ABAQUS User's Manual. Version Abaqus/CAE, p. 2021.
Abbass, A., Abid, S., Özakça, M., 2019. Experimental investigation on the effect of steel fibers on the flexural behavior and ductility of high-strength concrete hollow beams. Adv. Civ. Eng., 8390345
ACI Committee 239, 2012. Ultra-high Performance Concrete. ACI Fall Convention, Toronto, Ontario, Canada.
AFGC, 2013. Ultra High Performance Fibre-Reinforced Concretes. Interim Recommendations, Association Française de Génie Civil (AFGC) publication, Bagneux, France.
Ashour, S.A., 2000. Effect of compressive strength and tensile reinforcement ratio on flexural behavior of high-strength concrete beams. Eng. Struct. 22 (5), 413–423.
Ashour, S.A., Wafa, F.F., 1993. Flexural behavior of high-strength fiber reinforced concrete beams. ACI Struct. J. 90 (3), 279–287.
Chen, S., Zhang, R., Jia, L.J., Wang, J.Y., 2018. Flexural behaviour of rebar-reinforced ultra-high-performance concrete beams. Mag. Concr. Res. 70 (19), 997–1015.
Espion, B., 1994. Discussion of "flexural analysis of reinforced concrete beams containing steel fibers" by Byung Hwan Oh (October, 1992, vol. 118, No. 10). J. Struct. Eng. 120 (6), 1932–1934.
Feng, Z., Li, C., Yoo, D.Y., Pan, R., He, J., Ke, L., 2021. Flexural and cracking behaviors of reinforced UHPC beams with various reinforcement ratios and fiber contents. Eng. Struct. 248, 113266.
Feng, Z., Li, C., Ke, L., Yoo, D.Y., 2022. Experimental and numerical investigations on flexural performance of ultra-high-performance concrete (UHPC) beams with wet joints. Structures 45, 199–213.
Huang, H., Gao, X., Li, L., Wang, H., 2018. Improvement effect of steel fiber orientation control on mechanical performance of UHPC. Construct. Build. Mater. 188, 709–721.
Hung, C.C., Chueh, C.Y., 2016. Cyclic behavior of UHPFRC flexural members reinforced with high-strength steel rebar. Eng. Struct. 122, 108–120.
JSCE, 2008. Recommendations for Design and Construction of High Performance Fiber Reinforced Cement Composites with Multiple Fine Cracks (HPFRCC). Japan Society of Civil Engineers, Japan.
Lee, S.C., Cho, J.Y., Vecchio, F.J., 2011. Diverse embedment model for steel fiber-reinforced concrete in tension: model development. ACI Mater. J. 108 (5), 516–525.
Martinie, L., Lataste, J.F., Roussel, N., 2015. Fiber orientation during casting of UHPFRC: electrical resistivity measurements, image analysis and numerical simulations. Mater. Struct. 48 (4), 947–957.
Meng, S., Jiao, C., Ouyang, X., Niu, Y., Fu, J., 2022. Effect of steel fiber-volume fraction and distribution on flexural behavior of Ultra-high performance fiber reinforced concrete by digital image correlation technique. Construct. Build. Mater. 320, 126281.
Monte, F.L., Repesa, L., Snoeck, D., Doostkami, H., Roig-Flores, M., Jackson, S.J., Alvarez, A.B., Nasner, M., Borg, R.P., Schröfl, C., Giménez, M., Alonso, M.C., Serna, P., De Belie, N., Ferrara, L., 2024. Multi-performance experimental assessment of autogenous and crystalline admixture-stimulated self-healing in UHPFRCCs: Validation and reliability analysis through an inter-laboratory study. Cem. Concr. Compos. 145, 105315.
Naaman, A.E., 2003. Engineered steel fibers with optimal properties for reinforcement of cement composites. J. Adv. Concr. Technol. 1 (3), 241–252.
Naaman, A.E., Reinhardt, H.W., 2006. Proposed classification of HPFRC composites based on their tensile response. Mater. Struct. 39 (5), 547–555.
Oh, B.H., 1992. Flexural analysis of reinforced concrete beams containing steel fibers. J. Struct. Eng. 118 (10), 2821–2835.
Park, R., 1988. Ductility evaluation from laboratory and analytical testing. In: Proceedings of the 9th World Conference on Earthquake Engineering, vol. 8. Tokyo-Kyoto Japan, pp. 605–616.
Pyo, S., Wille, K., El-Tawil, S., Naaman, A.E., 2015. Strain rate dependent properties of ultra high performance fiber reinforced concrete (UHP-FRC) under tension. Cem. Concr. Compos. 56, 15–24.
Qiu, M., Shao, X., Wille, K., Yan, B., Wu, J., 2020. Experimental investigation on flexural behavior of reinforced ultra high performance concrete low-profile T-beams. Int. J. Concr. Struct. Mater. 14 (1), 1–20.
Qiu, M., Hu, Y., Shao, X., Zhu, Y., Li, P., Li, X., 2022. Experimental investigation on flexural and ductile behaviors of rebar-reinforced ultra-high-performance concrete beams. Struct. Concr. 23, 1533–1554.
Richard, P., Cheyrezy, M., 1995. Composition of reactive powder concretes. Cement Concr. Res. 25 (7), 1501–1511.
Ronanki, V.S., Aaleti, S., Valentim, D.B., 2018. Experimental investigation of bond behavior of mild steel reinforcement in UHPC. Eng. Struct. 176, 707–718.
Saqif, M.A., Tai, Y.S., El-Tawil, S., 2022. Experimental and computational evaluation of the ductility of UHPC beams with low steel-reinforcement ratios. J. Struct. Eng. 148 (7), 04022077.
Sawicki, B., Brühwiler, E., Denarié, E., 2022. Inverse analysis of R-UHPFRC beams to determine the flexural response under service loading and at ultimate resistance. J. Struct. Eng. 148 (2), 04021260.
Shao, Y., Billington, S.L., 2022. Impact of UHPC tensile behavior on steel reinforced UHPC flexural behavior. J. Struct. Eng. 148 (1), 04021244.
Shao, Y., Ostertag, C.P., 2022. Bond-slip behavior of steel reinforced UHPC under flexure: experiment and prediction. Cem. Concr. Compos. 133, 104724.
Shin, S.W., Ghosh, S.K., Moreno, J., 1989. Flexural ductility of ultra-high-strength concrete members. ACI Struct. J. 86 (4), 394–400.
Song, P.S., Hwang, S., 2004. Mechanical properties of high-strength steel fiber-reinforced concrete. Construct. Build. Mater. 18 (9), 669–673.
Soulioti, D.V., Barkoula, N.M., Paipetis, A., Matikas, T.E., 2011. Effects of fibre geometry and volume fraction on the flexural behaviour of steel-fibre reinforced concrete. Strain 47, 535–541.
Wille, K., Naaman, A.E., 2012. Pullout behavior of high-strength steel fibers embedded in ultra-high-performance concrete. ACI Mater. J. 109 (4), 479–488.
Wille, K., Kim, D.J., Naaman, A.E., 2011. Strain-hardening UHP-FRC with low fiber contents. Mater. Struct. 44 (3), 583–598.
Wille, K., El-Tawil, S., Naaman, A.E., 2014. Properties of strain hardening ultra high performance fiber reinforced concrete (UHP-FRC) under direct tensile loading. Cem. Concr. Compos. 48, 53–66.
Yang, I.H., Joh, C., Kim, B.S., 2010. Structural behavior of ultra high performance concrete beams subjected to bending. Eng. Struct. 32 (11), 3478–3487.
Yang, I.H., Park, J., Bui, T.Q., Kim, K.C., Joh, C., Lee, H., 2020. An experimental study on the ductility and flexural toughness of ultrahigh-performance concrete beams subjected to bending. Materials 13 (10), 2225.
Yang, J., Chen, B., Nuti, C., 2021. Influence of steel fiber on compressive properties of ultra-high performance fiber-reinforced concrete. Construct. Build. Mater. 302, 124104.
Yoo, D.Y., Moon, D.Y., 2018. Effect of steel fibers on the flexural behavior of RC beams with very low reinforcement ratios. Construct. Build. Mater. 188, 237–254.
Yoo, D.Y., Yang, J.M., 2018. Effects of stirrup, steel fiber, and beam size on shear behavior of high-strength concrete beams. Cem. Concr. Compos. 87, 137–148.
Yoo, D.Y., Yoon, Y.S., 2015. Structural performance of ultra-high-performance concrete beams with different steel fibers. Eng. Struct. 102, 409–423.
Yoo, D.Y., Yoon, Y.S., 2017. Bond behavior of GFRP and steel bars in ultra-high-performance fiber-reinforced concrete. Adv. Compos. Mater. 26 (6), 493–510.
Yoo, D.Y., Kang, S.T., Yoon, Y.S., 2014a. Effect of fiber length and placement method on flexural behavior, tension-softening curve, and fiber distribution characteristics of UHPFRC. Construct. Build. Mater. 64, 67–81.
Yoo, D.Y., Shin, H.O., Yang, J.M., Yoon, Y.S., 2014b. Material and bond properties of ultra high performance fiber reinforced concrete with micro steel fibers. Compos. Part B-Eng. 58, 122–133.
Yoo, D.Y., Kwon, K.Y., Park, J.J., Yoon, Y.S., 2015a. Local bond-slip response of GFRP rebar in ultra-high-performance fiber-reinforced concrete. Compos. Struct. 120, 53–64.
Yoo, D.Y., Zi, G., Kang, S.T., Yoon, Y.S., 2015b. Biaxial flexural behavior of ultra-high-performance fiber-reinforced concrete with different fiber lengths and placement methods. Cem. Concr. Compos. 63, 51–66.
Yoo, D.Y., Banthia, N., Yoon, Y.S., 2016a. Flexural behavior of ultra-high-performance fiber-reinforced concrete beams reinforced with GFRP and steel rebars. Eng. Struct. 111, 246–262.
Yoo, D.Y., Banthia, N., Kang, S.T., Yoon, Y.S., 2016b. Effect of fiber orientation on the rate-dependent flexural behavior of ultra-high-performance fiber-reinforced concrete. Compos. Struct. 157, 62–70.
Yoo, D.Y., Kang, S.T., Banthia, N., Yoon, Y.S., 2017a. Nonlinear finite element analysis of ultra-high-performance fiber-reinforced concrete beams. Int. J. Damage Mech. 26 (5), 735–757.
Yoo, D.Y., Yuan, T., Yang, J.M., Yoon, Y.S., 2017b. Feasibility of replacing minimum shear reinforcement with steel fibers for sustainable high-strength concrete beams. Eng. Struct. 147, 207–222.
Zhou, B., Uchida, Y., 2017. Influence of flowability, casting time and formwork geometry on fiber orientation and mechanical properties of UHPFRC. Cement Concr. Res. 95, 164–177.
Zhou, J., Li, C., Feng, Z., Yoo, D.Y., 2022. Experimental investigation on torsional behaviors of ultra-high-performance fiber-reinforced concrete hollow beams. Cem. Concr. Compos. 129, 104504.